Evolving Earth 1 (2023) 100013

Contents lists available at ScienceDirect

Evolving Earth

journal homepage: www.sciencedirect.com/journal/evolving-earth

# The link between lithospheric scale deformations and deep fluid emanations: Inferences from the Southeastern Carpathians, Romania

T.P. Lange [a,b,c,d,*], L. Palcsu [e], A. Szakács [f], Á. Kővágó [b,g], O. Gelencsér [b,c], Á. Gál [h], S. Gyila [i], T. M. Tóth [j], L. Mațenco [k], Cs. Krézsek [l], L. Lenkey [m], Cs. Szabó [a,b], I.J. Kovács [a,d]

[a] Institute of Earth Physics and Space Science, HUN-REN, Budapest, Hungary
[b] Lithosphere Fluid Research Lab, Institute of Geography and Earth Sciences, Eötvös Loránd University, Budapest, Hungary
[c] Doctoral School of Environmental Sciences, Eötvös Loránd University, Budapest, Hungary
[d] MTA FI Lendület Pannon Lit$H_2$Oscope Research Group, Hungary
[e] Isotope Climatology and Environmental Research Centre, Institute for Nuclear Research (ATOMKI), Debrecen, Hungary
[f] Institute of Geodynamics, Romanian Academy, Bucharest, Romania
[g] Doctoral School of Earth Sciences, Eötvös Loránd University, Budapest, Hungary
[h] Department of Geology, Babeș-Bolyai University, Cluj-Napoca, Romania
[i] Dr. Benedek Géza Rehabilitation Hospital, Covasna, Romania
[j] Department of Mineralogy, Geochemistry and Petrology, University of Szeged, Hungary
[k] Department of Earth Sciences, Utrecht University, the Netherlands
[l] OMV Petrom, Bucharrest, Romania
[m] Department of Geophysics and Space Science, Institute of Geography and Earth Sciences, Eötvös Loránd University, Hungary

## ARTICLE INFO

*Keywords:*
Mantle degassing
Fluid migration
Carbon dioxide
Deep seated deformation zones
Southeastern Carpathians
Stable isotope

## ABSTRACT

Understanding the formation, migration and emanation of deep $CO_2$, $H_2O$ and noble gases (He–Ne) in deep-seated deformation settings is crucial to know the complex relationship between deep-originated fluids and lithospheric deformation. To gain a better insight into these phenomena, we studied the origin of $H_2O$, $CO_2$ and noble gases of gas-rich springs found in the Târgu Secuiesc Basin located in the southeasternmost part of the Carpathian-Pannonian region of Europe. This study area is one of the best natural examples to understand the connection between the deep sources of gas emanations and deep-seated deformation zones, providing an excellent analogue for regions with similar tectonic settings and fluid emanation properties. We studied the $\delta^2H$ and $\delta^{18}O$ stable isotopic ratios of the spring waters, and the $\delta^{13}C$, He and Ne stable isotopic ratio of the emanating $CO_2$-rich gases dissolved in the mineral spring waters in Covasna town and its vicinity. Based on the $\delta^2H$, $\delta^{13}C$, $\delta^{18}O$ stable isotopic ratios, the spring waters and the majority of the gases are released through two consecutive fluid infiltration events. The preservation of the metamorphic signal of the upwelling $H_2O$ is linked to the local groundwater flow and fault abundancy. Furthermore, the noble gas isotopic ratios show a high degree of atmospheric contamination in the dissolved water gasses that is most likely related to the local hydrogeology. Nevertheless, the elevated corrected helium stable isotopic ratios ($R_c$/Ra) of our filtered data suggest that part of the emanating gases have a potential upper mantle source component. Beneath the Southeastern Carpathians, mantle fluids can have multiple origin including the dehydration of the sinking slab hosting the Vrancea seismogenic zone, the local asthenospheric upwelling and the lithospheric mantle. The flux of the mantle fluids is enhanced by lithospheric scale deformation zones that also support the fluid inflow from the upper mantle into the lower crust. The upwelling $CO_2$–$H_2O$ mantle fluids may induce the release of crustal fluids by shifting $X(CO_2)$ composition of the pore fluid and, consequently, initiating decarbonisation and devolatilization metamorphic reactions as a result of carbonate and hydrous mineral destabilisation in the crust. Based on the p-T-$X(CO_2)$ conditions of calc-silicates and the local low geotherm, we emphasise the importance of the upwelling fluids in the release and upward migration of further $H_2O$ and $CO_2$ in the shallower lower and upper crust. We infer that migration of deep fluids may also play an important role in addition to temperature control on the generation of crustal fluids in deep-seated deformation zones.

* Corresponding author. Institute of Earth Physics and Space Science, HUN-REN, Sopron, Hungary.
*E-mail address:* lange.thomas@epss.hun-ren.hu (T.P. Lange).

https://doi.org/10.1016/j.eve.2023.100013
Received 7 October 2023; Accepted 7 October 2023
Available online 12 October 2023

## 1. Introduction

Fluid emanations in various geological settings are complex processes in terms of understanding the connection between the upper mantle and surface observations, and requires a multidisciplinary approach by combining geochemistry, geophysics and tectonic knowledge. Therefore, a robust approach for constraining the geological evolution in deep-seated deformation zones requires a combination between studying composition of emanating volatiles (e.g., Kerrick and Caldeira, 1998), the lithospheric heat and electrical conductivity (e.g., Upton et al., 2003), seismic wave attenuation (e.g., Petrescu et al., 2021), the tectonic evolution, including nappe stackings, fault geometry and exhumation (e.g., Reiners and Brandon, 2006; Merten et al., 2010) with analysing the petrologic and geochemical character of the mantle source releasing fluids into the overlying crust (e.g., Tari et al., 1997; Kovács et al., 2018). Several studies explored the $CO_2$ degassing in various deep-seated deformation settings (i.e., penetrating the lower crust and/or the upper mantle), such as the Eastern Anatolia (Mutlu et al., 2008), Southern Appenines (Chiodini et al., 2004; Buttitta et al., 2023), the Himalayas (e.g., Kerrick and Caldeira, 1998; Evans et al., 2008; Groppo et al., 2017, 2022), Alps and their vicinity (e.g., Bräuer et al., 2016), Southern Alps of New Zealand (e.g., Upton et al., 2000, 2003) and San Andreas Fault (e.g., Pili et al., 2011). These studies pointed out gas-rich springs along deep-seated deformation zones and proposed a mixed crustal and mantle origin for most of the emanating $CO_2$-rich gases. In addition, intense gas emanation can affect the habitat of terrestrial life (e.g., distribution of plants) and consequently is an important topic from a biogeodynamic point of view (Kusakabe et al., 1989; Jánosi et al., 2022). From a rheological perspective, the migration of deep fluids in a deep-seated ductile environment (mantle, lower crust) is controlled by the rate and speed of deformation (Sleep and Blanpied, 1992), whereas the fluid migration in the upper (brittle) crust is controlled by the permeability of the fluid-hosting rocks (e.g., Bense et al., 2013). The existence of fluids (e.g., $CO_2$, $H_2O$, noble gases) migrating throughout the lithosphere strongly depends on the chemical and physical properties of the source and hosting environments (e.g., Eh, pH, fluid composition, temperature; e.g., Manning et al., 2013). In the lithospheric mantle, pure $CO_2$ acts as an inert fluid (similar with noble gases) and its migration to the crust is considered spontaneous (e.g., Szabó and Bodnar, 1996; Vaselli et al., 2002; Frezzotti and Touret, 2014). In contrast, the behaviour of $CO_2$ in the crust is significantly more complex. Crustal $CO_2$ can be related to the decomposition of carbonates or to the oxidation of reductive carbon-bearing compounds (e.g., graphite, $CH_4$; Kerrick and Caldeira, 1998). Despite these extensive studies, the interaction between deeply sourced mantle fluids and crust, in releasing the observed $CO_2$ emanations in complex deep-seated deformation settings associated with actively sinking slabs, is less understood (e.g., Vaselli et al., 2002; Caracausi and Sulli, 2019; Groppo et al., 2022).

In the well-studied Carpathian-Pannonian region (CPR) of Central Europe numerous potential post-volcanic and mantle derived $CO_2$ emanating localities (mofettes, springs) were observed in volcanic and non-volcanic areas (Vaselli et al., 2002; Bräuer et al., 2016; Sóki and Csige, 2016; Kis et al., 2019, 2020). One of the best-known localities is

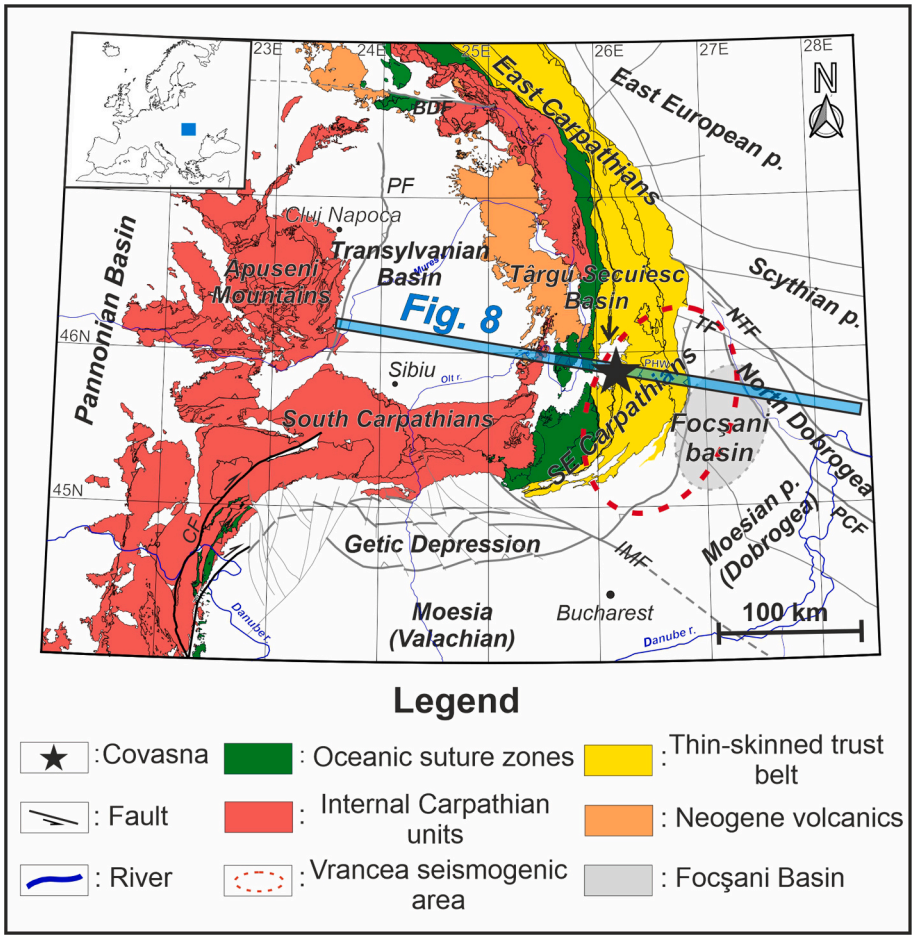


**Fig. 1.** Simplified tectonic map showing the main units of the Eastern, Southern Carpathians and the Southeastern Carpathians (simplified and modified after Mațenco, 2017; Kovács et al., 2021). IMF = Intra-Moesian Fault; TF = Trotuș Fault; NTF = New Trotuș Fault; PCF = Peceneaga-Camena Fault; BDF – Bogdan Vodă – Dragos Vodă faults system; PF – Puini Fault; CF – Cerna Fault; PHW – Putna Half-Window.

the town of Covasna, located in the southeastern part of the Târgu Secuiesc Basin, in the intramountain hinterland area of the Southeastern Carpathians (Fig. 1). The $\delta^{13}C$ stable isotopic ratios of $CO_2$ and associated helium isotopic ratios ($R/R_a$) of springs from the Târgu Secuiesc Basin and surrounding areas assume a different source than the classically presumed "post-volcanic derived" emanations in the nearby Harghita Mountains (Vaselli et al., 2002). These authors also suggested that the $CO_2$-rich gases of the Târgu Secuiesc Basin and surrounding area are most likely linked to the thermal/hydrothermal decomposition of subducted crustal carbonates followed by mixing with upper mantle fluids. Despite this important pioneering approach, the exact source of the crustal gases is still not known, whether they originate from the decarbonation of carbonates within the nearby sinking Vrancea slab or from the middle and lower crust of the overlying Moesian platform.

Therefore, we aim to study the correlation between mantle and crustal sources in the release of $H_2O$ and $CO_2$ emanations in a deep-seated deformation setting by building a fluid evolution model using the latest geochemical, geophysical and tectonic results acquired for the Southeastern Carpathian region. To derive process-oriented conclusions, we furthermore compare our model with other regional settings that contain deep-seated deformation zones, following previous inferences in correlating fluid flows with deformation. The joint study of isotopic ratios of water and dissolved gases (particularly $CO_2$ and noble gases) in the $CO_2$-rich springs located in the area of Covasna town provides a good opportunity to understand the evolution of the volatiles in a tectonically active, extinct volcanic area, used as a comparison with other volcanic and non-volcanic $CO_2$ emanation areas.

## 2. Geological background

The Carpathian orogen, including its bend area was ultimately established during the post-Paleogene convergence and collision between the internal Carpathian units and the Moesian and European platforms (Fig. 1), followed by vertical movements associated with the continued retreat and steepening of the Vrancea slab (Maţenco, 2017). In the Southeastern Carpathians, the Cretaceous Ceahlău-Severin oceanic unit was sutured at the collision contact eastwards with an external thin-skinned east-verging thrust belt that was deformed during latest Paleogene – Miocene times until around 8 Ma (Fig. 1; Bădescu, 2005; Maţenco et al., 2010). This structuration was followed by differential vertical movements characterized by subsidence in the Focşani Basin foreland and uplift in the orogenic wedge, associated with limited extension and the formation of Pliocene – Quaternary intramountain basins, such as the Braşov and Târgu Secuiesc basins (Girbacea and Frisch, 1998; Ciulavu et al., 2000; Merten et al., 2010; Necea et al., 2021). The foreland basin subsidence was driven by the downward pull of the actively sinking slab associated with the Vrancea seismogenic zone, mapped by teleseismic tomography (100•70•30 km, Martin et al., 2006; Radulian et al., 2008). This seismogenic zone is characterized by strong ($M_w > 6$) intermediate depth mantle (~70–170 km) and crustal earthquakes, associated with asthenospheric upwelling in the hinterland of the orogen, interpreted to reflect active detachment and/or delamination processes (Tondi et al., 2009; Göğüş et al., 2016; Petrescu et al., 2021; Ferrand and Manea, 2021; Kovács et al., 2021). The NW-most termination of the crustal and mantle earthquakes hypocentres are located beneath the SE corner of the intramountain (Braşov and Târgu Secuiesc) basins (Ferrand and Manea, 2021). The subduction and collision were also associated with a NNW-SSE oriented calc-alkaline to ultrapotassic alkaline volcanism that took place along the Călimani-Gurghiu-Harghita volcanic chain (10.5–0.03 Ma) at the interior of the Eastern Carpathians (Fig. 1; Szakács and Seghedi, 1995; Fielitz and Seghedi, 2005; Pécskay et al., 2006; Seghedi et al., 2019). During the last stages of magmatism, the southern end of the Călimani-Gurghiu-Harghita volcanic chain changed gradually its character to adakitic-like and K-alkaline, well studied in the southern Harghita mountains (~1.96–0.03 Ma; Pécskay et al., 2006; Szakács et al., 2015; Molnár et al., 2018). Simultaneously with the volcanic activity of the southern Harghita Mountains, alkali basaltic volcanism took place in the Perşani Mountains Volcanic Field (1.2–0.6 Ma; Downes et al., 1995; Panaiotu et al., 2013; Seghedi et al., 2016), exposing abundant lithospheric mantle xenoliths from an enriched, highly deformed lithospheric mantle source (Vaselli et al., 1995; Falus et al., 2000, 2008; Kis et al., 2019; Molnár et al., 2021; Faccini et al., 2020). No volcanic activity occurred in the Southeastern Carpathians and its vicinity in the last ~28 ka, after the most recent volcanic activity ceased (Karátson et al., 2019), yet $CO_2$ degassing defined as 'post-volcanic' is still observed in the Harghita Mountains and its closer and farther vicinity (Kis et al., 2019). In the Perşani Mountains Volcanic Field the degassing in the form of gas-rich springs is much less intense. Active surface $CO_2$ emanations are also observed along the older calc-alkaline Călimani and Gurghiu Neogene volcanic areas (e.g., Kis et al., 2020) and their neighbourhood where no volcanic activity occurred, such as Quaternary Borsec and Bilbor Basins along the eastern margin of the Transylvanian and other intramountain basins (Fielitz and Seghedi, 2005). Kis et al. (2020) distinguished two $CO_2$ emanation types along the eastern boundary of the Transylvanian Basin and in the Eastern Carpathians. One type is related to the methane released from the Middle Miocene (Badenian) salt diapirs, which is associated with NaCl-rich waters. The other type is the southward continuation of the Călimani-Gurghiu-Harghita volcanic chain ending in the Târgu Secuiesc Basin and is associated with $HCO_3^-$-rich water springs. In summary, these localities are part of the so-called 'mofette aureola' of the Neogene volcanic range. This area covers all active $CO_2$ emanation localities along the western margin of the Eastern Carpathians and in the eastern Transylvanian Basin, spread out over more than 13 000 $km^2$ (Airinei and Pricăjan, 1975). Springs found in the vicinity of the Târgu Secuiesc Basin are limited to its boundaries, potentially showing a relationship between their origin and marginal normal faults (e.g., Kis et al., 2020). This basin overlies the internal parts of the thin-skinned wedge (Audia and Tarcău nappes) that consist of dominant Cretaceous siliciclastic sediments (Fig. 2/a-b; Roban and Melinte-Dobrinescu, 2012). These thin-skinned nappes are thrusted over the Moesian platform that consists of Mesozoic to Palaeozoic carbonates and siliciclastic sediments overlying a Precambrian crystalline basement (Seghedi et al., 2005; Saintot et al., 2006).

Sub-surface hydrogeological water flow in the vicinity of Covasna town takes place by percolation through Cretaceous sediments of the neighbouring Carpathian nappes and directed towards the Târgu Secuiesc Basin (Bandrabur, 1962, 1967). These water flows are sometimes disrupted by smaller faults located at the basin boundary and intramountain valleys (Bandrabur, 1962). Hydrogeological drillings showed an increase in dissolved $CO_2$ concentration in the underground water in the vicinity of major faults. The dissolved $CO_2$ concentration positively correlates with the salinity of the underground waters (Bandrabur, 1967). In the northeastern part of Covasna town the total dissolved solid concentration reached particularly high values (>17 000 mg/l).

## 3. Methodology

### 3.1. Sampling of the spring waters and dissolved gases

In the larger area of the Covasna town, water and gas samples were collected from springs located in the Covasna Park (Elvira-1 and Elvira-2 springs; small spring adjacent to the Covasna creek; spring located behind the Kőrösi Csoma Sándor Lyceum), the Comandău Forestry Office courtyard, Benedek Géza Rehabilitation Hospital, and various springs within the Hankó valley (Fig. 2/b-d). Furthermore, one water sample was collected from the centre of Tamaşfalău village located ~5 km NW from Covasna situated in the Târgu Secuiesc Basin (Fig. 2b). We used this latter water sample to distinguish the stable isotopic ratio differences between the centre and boundary waters of the Târgu Secuiesc Basin. A detailed description of the sampling sites can be found

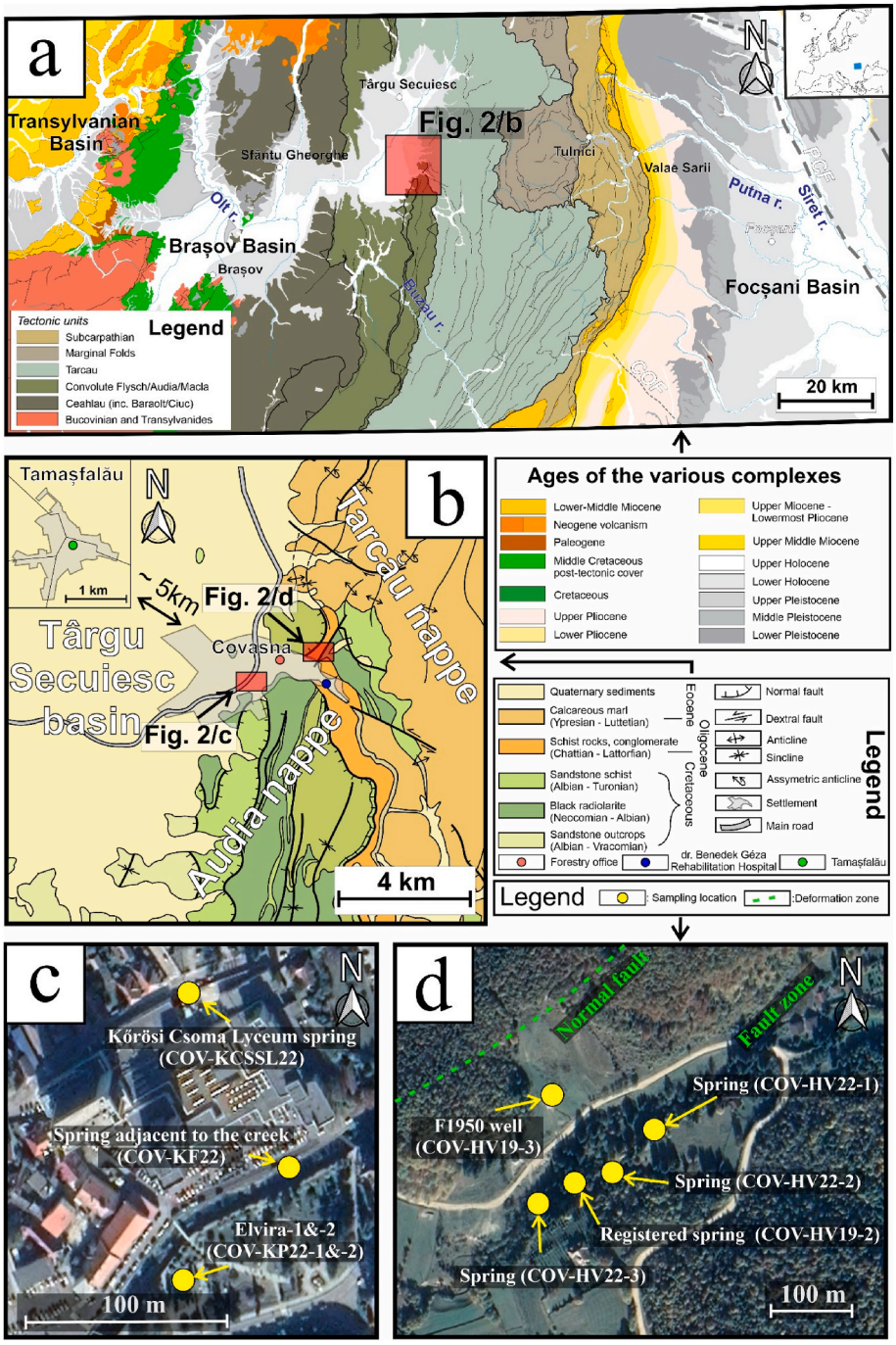


**Fig. 2.** a) Tectonic map of the Southeastern Carpathians showing the relationship between the thin-skinned nappes and the geology of the Brașov and Târgu Secuiesc Basins, as well as the adjacent Transylvanian Basin and foreland of the Southeastern Carpathians (slightly modified after Necea et al., 2021). PCF = Peceneaga-Camena Fault; COF = Capidava-Ovidiu Fault, TF = Trotus Fault. **b**) Local geological map of the Covasna town and surrounding area including Tamașfalău (modified after Murgeanu et al., 1968) showing the sampling locations. Figure **c** and **d** show the sampling locations (yellow circles) on Google maps images that are located in and near the Covasna Park and the Hankó valley (Voinești), respectively. The Comandău Forestry Office, Benedek Géza Rehabilitation Hospital and Tamașfalău sampling locations are indicated with red, blue and green circles in figure **b**, respectively, whereas yellow circle in figure **c** and **d** show the sampling locations within and near the Covasna Park and Hankó valley. (For interpretation of the references to colour in this figure legend, the reader is referred to the Web version of this article.)

in Supplementary Material 1.

Water samples were collected in cylindrical plastic containers. During water sampling the cylindrical plastic containers were filled underwater to prevent isotopic contamination with atmospheric air. Then the sample holders were stored at low temperature (<5 °C) to slow down microbiological processes.

Gas samples were extracted on-site from gas-rich spring waters using a portable device introduced and described in detail in Papp et al. (2016). The device is a 40•40•30 cm box with a metal plate on top carrying all the parts of the device that are connected via small metal tubes that are distributed in the following configuration. On one end of the metal plate, a membrane contactor (Liqui-Cel) is attached that has a water in- and outlet on both ends supporting the continuous water flow. The membrane contactor is built up with 7200 tiny polyurethane hollow

fiber tubes. Perpendicular to the water flow direction (i.e., towards the centre of the metal plate), metal tubes and metal ball valves connect the membrane contactor to one-one glass ampoule filled with silica gel. The glass ampoules are further attached onto a pressure gauge that is connected to a 'T' connector. The 'T' connector provides a connection to the external vacuum unit and the ~100 $cm^3$ sized stainless steel cylinder container (i.e., gas sample holder). The gas sample holder has two openings on both ends to provide gas in and outflow both ends equipped with a metal ball valve. The other end of the gas sample holder is connected to the circulator pump that is positioned inside the box of the portable device. Finally, the circulator pump is connected to the silica gel filled glass ampoule. A detailed description of the sampling procedure is found in Supplementary 2.

### 3.2. Water and gas composition and isotopic measurements

All bulk gas, stable isotopic and water conductivity measurements were performed at the Isotope Climatology and Environmental Research Centre (ICER), Institute of Nuclear Research (ATOMKI) in Debrecen (Hungary). The major gas composition ($N_2$, O, Ar, $CO_2$) were determined by quadrupole mass spectrometry (OmniStar, Pfeiffer Vacuum). Water samples for $\delta^2H$ and $\delta^{18}O$ were distilled and then measured using a LGR Liquid Water Isotope Analyser (model: 912–0050) with an accuracy of 0.5‰ and 0.15‰, respectively (Túri et al., 2020). Obtained values $\delta^2H$ and $\delta^{18}O$ were normalized for V-SMOW.

The measured isotopes from the extracted total gas samples are the following: $\delta^{13}C$ and $\delta^{18}O$ isotopic ratio of $CO_2$ and the $^3He$, $^4He$ and $^{20}Ne$ noble gas concentration. Values of $\delta^{13}C$ and $\delta^{18}O$ were measured using a Thermo Finnigan DELTA$^{PLUS}$ XP with an accuracy of ±0.1‰ for both elements. Helium was measured using a Thermo Scientific Helix SFT mass spectrometer, whereas Ne with a VG-5400 mass spectrometer. For each noble isotopic measurement, we used approximately 1 $cm^3$ of the collected gas. Prior to the measurements, we introduced the noble gases for 40 min first in a molecular sieve trap at liquid nitrogen temperature, and then into two cryogenic traps cooled at 25 K (empty trap, for Ar; Kr, Xe) and 10 K (charcoal trap, for He and Ne). During the measurement, He was first released from the trap at 42 K. After He measurements the trap chamber was heated to 90 K releasing the Ne gas from the charcoal traps. Background air measurement for He and Ne were conducted by measuring at the atmosphere of the laboratory at the same day of the measurements. Known-volume air aliquots were repeatedly run through in the same way on the gas purification line for the calculation of concentrations. Signals were collected by a Faraday cup in the case of $^4He$ and $^{20}Ne$ isotopes and by an electron multiplier for $^3He$. The helium blank was 1 × 10–10 ccSTP (ccSTP: cubic centimetre at standard temperature and pressure, 0 °C and 1 atm), whereas neon blank was 5 × 10–10 ccSTP. The analytical error of the measurements was 1.5–2.5% for $^3He$, <1% for $^4He$ and <5% for $^{20}Ne$, . Further details of the analytical procedure are available in Papp et al. (2012).

From the acquired $^3He/^4He$ and $^4He/^{20}Ne$ isotopic ratio results, we calculated the corrected $^3He/^4He$ ratios ($R_c/R_a$), more precisely, the $^3He/^4He$ ratio, which is free of atmospheric contamination. For this, we used the equation of Giggenbach et al. (1993):

$$R_c/R_a = ((R_m/R_a)\,(^4He/^{20}Ne)_m - (^4He/^{20}Ne)_a) / ((^4He/^{20}Ne)_m - (^4He/^{20}Ne)_a), \quad (1)$$

Where $R_m/R_a$ is the measured $^3He/^4He$ isotopic ratio, the $(^4He/^{20}Ne)_m$ is the measured $^4He/^{20}Ne$ isotopic ratio and the $(He/Ne)_a$ is the atmospheric air $^4He/^{20}Ne$ isotopic ratio dissolved in spring water. The dissolved atmospheric air $^4He/^{20}Ne$ isotopic ratio is equivalent to 0.274 for 5 °C degree waters. In the following, we will only discuss the $R_c/R_a$ ratios.

### 3.3. Calculation of temperature and depth curves for the Târgu Secuiesc Basin

To constrain the temperature conditions beneath the Târgu Secuiesc Basin, we calculated the temperature-depth distribution assuming a one-dimensional steady-state model (e.g., Chapman and Furlong, 1992):

$$T_i = T_{i0} + \frac{q_{i0}}{k_i}\Delta z - \frac{A_i}{2k_i}\Delta z^2 \quad (2)$$

where $T_i$ is the temperature at depth $\Delta z$ in layer $i$, $k_i$ and $A_i$ are the thermal conductivity and heat production rate in layer $i$, respectively, and $T_{i0}$ and $q_{i0}$ are temperature and heat flow density at the top of the layer, respectively. We considered the temperature dependence of the thermal conductivity applying the laws described in Vosteen and Schellschmidt (2003).

The layers in Equation (2) are in accordance with the crustal structure. The crustal structure is well known in the study area because the VRANCEA2001 deep seismic refraction profile (Hauser et al., 2007) coincides with the section shown in Fig. 1. The crustal structure and the thermal parameters are given in Table 1. The upper crust is built up of Paleogene and older sedimentary rocks units (including thin-skinned nappes and upper part of the Moesian microplate). The middle crust is granitic and granodioritic in composition whereas the lower crust is composed of gneiss and amphibolite (Hauser et al., 2007). The thermal conductivities and heat production rates are in line with the composition of the crust (Cermák, 1993) and agree with the values used by Andreescu et al. (2002) and Tiliță et al. (2018) who modelled crustal temperature distribution in the Transylvanian Basin. We estimated the effect of the uncertainty of the thermal parameters in the upper crust on the temperature-depth function. The mean values are characteristic for an average sedimentary rock composition; shaly and clayey sediments are characterized by lower thermal conductivity and higher heat production rate relative to the mean values, while sandstones and carbonates have higher thermal conductivity and lower heat production rate. The temperature was calculated in the case of these two endmember lithologies, too. Variation of the middle and lower crustal thermal parameters do not affect the temperature in the upper crust, therefore only the mean values were used (Table 1).

As the surface heat flow in the study area is generally moderate to low (40–45 $mW/m^2$; Veliciu and Demetrescu, 1979; Demetrescu and Veliciu, 1991; Hurtig et al., 1992; Andreescu and Demetrescu, 2001; Tiliță et al., 2018) we carried out the calculation for these values.

## 4. Results

### 4.1. Isotopic ratio of the spring waters

The measured $\delta^2H$ and $\delta^{18}O$ isotopic ratios of the gas-rich spring waters are expressed in permil (‰) versus SMOW (Standard Mean Ocean Water) and are presented in Table 2. Water samples from the Elvira-1 spring, the spring adjacent to the Covasna creek, the spring located behind the Kőrösi Csoma Sándor Lyceum, the Comandău Forestry Office (Voinești) and one of the spring located in the Hankó valley (COV-HV22-

**Table 1**
Thermal parameters used in the calculation of the crustal temperature. Thermal conductivity is measured on 20 °C. The depth of the crust is based on Hauser et al. (2007), the thermal conductivity and heat production rates were taken from Vosteen and Schellschmidt (2003).

| | Depth (km) | Thermal conductivity (W/m/K) | Heat production rate (10-6 W/$m^3$) |
|---|---|---|---|
| Upper crust | 17 | 2.7 | 1 |
| Middle crust | 27 | 3.1 | 1.5 |
| Low velocity zone | 35 | 3.1 | 0.2 |

**Table 2**
$\delta^2H$ and $\delta^{18}O$ isotopic ratios, water conductivity together with the coordinates of the sampling localities. StDev = Standard Deviation.

| Location | Sample code | $\delta^2H$ | $\delta^2H$ StDev | $\delta^{18}O$ | $\delta^{18}O$ StDev | Water conductivity (μS) | Coordinates |
|---|---|---|---|---|---|---|---|
| Tamaşfalău | SZTF22 | −93.94 | 0.37 | −12.44 | 0.082 | 2350 | 45°53′03.5″N 26°07′00.3″E |
| Comandău Forestry Office (Covasna) | COV–F22 | −69.74 | 0.34 | −9.71 | 0.069 | 880 | 45°51′10.9″N 26°11′19.6″E |
| Kőrösi Csoma Sándor Lyceum | COV-KCSSL22 | −71.51 | 0.43 | −8.93 | 0.085 | 1808 | 45°50′48.7″N 26°10′10.1″E |
| Adjacent to the Covasna creek | COV-KISF22 | −74.29 | 0.42 | −10.11 | 0.082 | 643 | 45°50′43.1″N 26°12′33.9″E |
| Elvira-1 spring (carbonated water) | COV-KP22-1 | −69.77 | 0.36 | −8.40 | 0.058 | 1098 | 45°50′43.3″N 26°10′10.3″E |
| Elvira-2 spring (salty water) | COV-KP22-2 | −63.23 | 0.37 | −6.82 | 0.084 | 6160 | 45°50′43.3″N 26°10′10.3″E |
| Benedek Géza Rehabilitation Hospital | COV-BGRH22 | −39.53 | 0.04 | 6.18 | 0.042 | 17 800 | 45°50′43.1″N 26°12′33.9″E |
| Hankó valley (Registered spring) | COV-HV19-2 | −51.01 | 0.26 | 1.49 | 0.064 | 12 200 | 45°51′12.2″N 26°12′18.4″E |
| Hankó valley (F1950 drill) | COV-HV19-3 | −33.87 | 0.26 | 9.11 | 0.084 | 10 200 | 45°51′14.7″N 26°12′17.7″E |
| Hankó valley (NE Bath) | COV-HV22-1 | −52.70 | 0.27 | −2.41 | 0.077 | 1449 | 45°51′14.2″N 26°12′24.5″E |
| Hankó valley (SW Bath) | COV-HV22-2 | −71.57 | 0.26 | −10.26 | 0.060 | 665 | 45°51′13.3″N 26°12′22.1″E |
| Hankó valley (small pond) | COV-HV22-3 | −44.32 | 0.50 | 3.12 | 0.068 | 2300 | 45°51′14.7″N 26°12′17.7″E |

2) (Fig. 3) show similar isotopic ratio ($\delta^2H \sim -70.0‰$, $\delta^{18}O \sim -9.0‰$). The $\delta^2H$ and $\delta^{18}O$ isotopic ratios of these waters coincides with the local meteoric water line determined by Ionete et al. (2015). Compared these springs to the other Hankó valley springs, the spring of the Benedek Géza Rehabilitation Hospital, the Elvira-2 salty water spring show more positive δ-values. The distribution of these values on a $\delta^2H$ vs. $\delta^{18}O$ diagram show a strong positive ($R^2 = 0.98$) correlation (Fig. 3). The COV-HV19-3 sample presents the end of the local trendline ($\delta^2H = -44.3‰$ and $\delta^{18}O = +3.12‰$) (Fig. 3). The trendline is less steep and, therefore, differs from the evaporation trendline presented by Vaselli et al. (2002). The spring, located in the centre of Tamaşfalău, shows lower δ-values compared to those of Covasna spring waters and also fell on the local meteoric water line.

### 4.2. Gas composition

The concentration of $CO_2$, atmospheric components ($N_2$, $O_2$ and Ar)

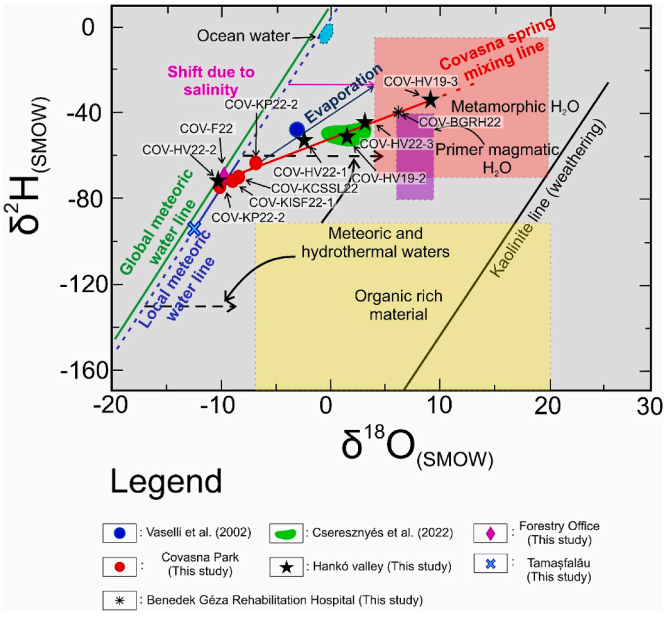


**Fig. 3.** Variation of $\delta^2H$ vs. $\delta^{18}O$ stable isotopic ratio plot after Sheppard (1986), and Yardley and Bodnar (2014) also showing the evaporation line (Vaselli et al., 2002), local meteoric water line (Ionete et al., 2015; Rozanski et al., 2013) and global meteoric water line (Rozanski et al., 2013). The studied spring water samples create a Covasna spring mixing water line. For comparison, published data on the Elvira spring (Elvira-1 spring; Vaselli et al., 2002) and $\delta^2H$ and $\delta^{18}O$ range of the 'Registered' spring in the Hankó valley (Cseresznyés et al., under review) are also presented. The water sample of Tamaşfalău falls onto the local meteoric water line, but at a different position than the Covasna spring waters. SMOW = Standard Mean Ocean Water.

and noble gases (He and Ne) of the sampled dissolved gases are shown in Table 3. High compositional variability of the atmosphere components and $CO_2$ can be observed. Sample COV-HV22-3 has the lowest $CO_2$ (43.6%) and highest $N_2$ (44.6%) concentration, whereas sample COV-HV22-1 has the highest $CO_2$ (80.7%) and lowest $N_2$ (17.1%) concentration. In contrast, He and Ne concentrations, excluding sample COV-HV22-3, show very similar and low composition (He: 0.88–2.15 ppm and Ne: 1.8–7.81 ppm). In COV-HV22-3 sample, the increase of these noble gas concentration (He: 2.67 ppm and Ne: 10.74 ppm) is observed compared to the other samples along with the highest quantity of atmospheric component (Table 3).

### 4.3. Isotopic ratios of the gases

The measured $\delta^{13}C$ and $^3He/^4He$ isotopic ratios of the gas-rich spring extracted samples are shown in **Table 4**. The $\delta^{13}C$ isotopic ratios of the dissolved $CO_2$ are expressed in permil (‰) versus the V-PDB (Vienna Pee Dee Belemnite) and form a narrow range between −2.0‰ and −0.47‰ (Table 4). No relation between the $\delta^{13}C$ isotopic ratios and the $CO_2$ concentration can be seen. The $\delta^{13}C$ isotopic ratios show a weak negative correlation with the $\delta^2H$ ($R^2 = 0.25$) and $\delta^{18}O$ ($R^2 = 0.29$) isotopic ratios of the spring waters.

The measured $^3He/^4He$ isotopic ratios of the collected gas samples (expressed in $R/R_a$; sample $^3He/^4He$ divided by the atmospheric $^3He/^4He$; Marty and Zimmermann, 1999) show narrow range ($R/R_a$ = 1.54–1.55) with one outlier (COV-HV19-3; $R/R_a = 1.42$). All measured samples have very low $^4He/^{20}Ne$ values (0.27–0.72; Table 4) that were used during atmospheric correction calculations (equation (1)). The low $^4He/^{20}Ne$ isotopic ratios will result in higher uncertainty. The corrected helium isotopic ratios ($R_c/R_a$) show a wider range in helium isotopic ratios. From these data only three values are satisfactory (COV-HV22-1, COV-HV22-2 and COV-KP22-1) and show a range of $R_c/R_a$ = 1.88–2.45 (Table 4). The error of the satisfactory $R_c/R_a$ isotopic ratios was ±0.13. No correlation between the $\delta^{13}C$ isotopic ratios and $R_c/R_a$ can be observed. In contrast, the $R_c/R_a$ isotopic ratios show strong positive

**Table 3**
Chemical composition of the sampled Covasna gases. NA = not analysed, ppm = parts per million.

| Sampling site | Sample name | $N_2$ (%) | $O_2$ (%) | Ar (%) | $CO_2$ (%) | He (ppm) | Ne (ppm) |
|---|---|---|---|---|---|---|---|
| Hankó valley (NE bath) | COV-HV22-1 | 17.1 | 2.03 | 0.18 | 80.7 | 1.85 | 4.68 |
| Hankó valley (SW bath) | COV-HV22-2 | 17.1 | 4.60 | 0.21 | 78.1 | 2.15 | 3.30 |
| Hankó valley (small pond) | COV-HV22-3 | 44.1 | 11.8 | 0.53 | 43.6 | 2.67 | 10.7 |
| Elvira-1 spring (carbonated water) | COV-KP22-1 | 28.5 | 7.65 | 0.34 | 63.5 | 0.88 | 1.80 |
| Hankó valley (F1950 drill) | COV-HV19-3 | NA | NA | NA | NA | 1.17 | 4.67 |

**Table 4**
Stable isotopic ratios of the sampled Covasna gases. $R/R_a$ and $R_c/R_a$ are the measured and corrected $^3He/^4He$ isotopic ratios of the sampled Covasna gases, respectively.

| Sample | Sampling site | $\delta^{13}C$ | $R/R_a$ | $^4He/^{20}Ne$ | $R_c/R_a$ (satisfactory) | $R_c/R_a$ (discarded) |
|---|---|---|---|---|---|---|
| COV-HV22-1 | Hankó valley (NE bath) | −0.77 | 1.54 | 0.44 | 2.45 | – |
| COV-HV22-2 | Hankó valley (SW bath) | −1.37 | 1.55 | 0.72 | 1.88 | – |
| COV-HV22-3 | Hankó valley (small pond) | −0.84 | 1.52 | 0.27 | – | 196.79 |
| COV-KP22-1 | Elvira-1 spring (carbonated water) | −0.55 | 1.54 | 0.54 | 2.10 | – |
| COV-HV19-3 | Hankó valley (F1950 drill) | −2.00 | 1.41 | 0.28 | – | 46.23 |

correlation with $\delta^2H$ ($R^2 = 0.91$) and $\delta^{18}O$ ($R^2 = 0.97$) isotopic ratios of the spring waters.

## 5. Discussion

### 5.1. Spatial distribution of the water and gas isotopic ratios

#### 5.1.1. Water isotopic ratios

The similar $\delta^2H$ and $\delta^{18}O$ isotopic ratios of the studied waters from the Covasna Park and surrounding area, Forestry Office and the COV-HV22-2 sample from the Hankó valley fall onto the local meteoric water line and, therefore, they reflect the local groundwater composition (Fig. 3). Similarly to these springs, the spring of Tamașfalău falls onto the local meteoric water line yet has lower $\delta^2H$ and $\delta^{18}O$ isotopic ratios compared to the Covasna spring waters. The isotopic ratios of the Hankó valley (COV-HV19-2,3, COV-HV22-1,3) and the Benedek Géza Rehabilitation Hospital (COV-BGRH11) spring samples define a mixing line between the local meteoric waters (described above) and what is generally thought to reflect metamorphic waters (Evans et al., 2008). This mixing line differs from the evaporation trendline proposed by Vaselli et al. (2002) (Fig. 3). The difference is owed to the kinetic fractionation that occurs during evaporation, whereas this process is absent during subsurface fluid mixing. Based on the isotopic ratios of the sampled springs (Table 2), a continuous enrichment in heavy isotopes ($^2H$, $^{18}O$) can be observed from the Târgu Secuiesc Basin (i.e., Tamașfalău) towards the boundary with the Southeastern Carpathians (e.g., Hankó valley, Benedek Géza Rehabilitation Hospital). This trend is most likely linked with the topographically controlled westward underground water flow and eastward increase in fault frequency from the Târgu Secuiesc Basin towards its margin (Bandrabur, 1962). Therefore, spring waters at more elevated topographic positions (e.g., Hankó valley; ~625 m) have more significant metamorphic isotopic signature than the springs located at lower topographic levels (e.g., Covasna Park and adjacent springs; ~570 m, see also Bandrabur, 1962). The metamorphic end member of the Hankó valley spring water (COV-HV19-3) originates from ~180 m depth (F1950 drill) that corresponds to the deeper groundwater levels (Bandrabur, 1962), where only a slight isotopic overprint by the groundwater can occur. Csereszynés et al. (under review) measured repeatedly the isotopic ratios of the COV-HV19-2 registered spring located nearby the F1950 drill in the Hankó valley to study the seasonal variance and concluded that the $\delta^2H$ and $\delta^{18}O$ stable isotopic ratios of these waters are quasi constant in time with an average of $\delta^2H = -49.7$ (±0.8) and $\delta^{18}O = +2.0$ (±0.8) (Fig. 3). As the other Hankó valley springs (e.g., the F1950 drill) lie along the same fault as the COV-HV19-2 spring, it is likely that their $\delta^2H$ and $\delta^{18}O$ isotopic ratios show a similar constant isotopic ratio over time allowing us discard seasonal influence, at least in the investigated time period in all samples from the valley.

#### 5.1.2. Gas isotopic ratios

The quasi homogenous $\delta^{13}C$ isotopic ratios of Covasna gases (Table 4) suggest the same fluid evolution of the Covasna gases, whereas the large variability of $\delta^{18}O$ assumes an isotopic exchange between $H_2O$ and $CO_2$. Considering the observed small variations of the $\delta^{13}C$ isotopic ratio, the elevated dissolved $CO_2$ concentration (43.6–80.7%; Table 3) is more than sufficient to preserve their original values (Bräuer et al., 2014), regardless of numerous other processes that may cause fractionation of $\delta^{13}C$ isotopic ratio in the $CO_2$ gas (Mook and Rozanski, 2000; Gwénaëlle Chaillou et al., 2014; Csereszynés et al., under review). Elevated corrected helium isotopic ratios ($R_c/R_a$) (**Table 4**) suggest a deep origin for the upwelling fluids because elevated $^3He$ ratios cannot originate from surface or subsurface processes (Niedermann, 2002). Furthermore, the high dissolved atmospheric air ($N_2$, $O_2$, Ar) content of some spring waters (Table 3) support a high atmospheric contamination that is also reflected by the low $^4He/^{20}Ne$ isotopic ratio (**Table 3**). As the water pump was always underwater during the dissolved gas sampling, it is logical to assume that the atmospheric contamination occurred during the subsurface shallow water mixing between the upwelling fluids and air-saturated groundwater.

### 5.2. The origin of the covasna water and gases

#### 5.2.1. Upper mantle fluids

The Covasna noble gases have an elevated $^3He$ concentration ($R_c/R_a$ = 1.88–2.44; **Table 2**) suggesting contributions of mantle fluids to the overall isotopic signature. These $R_c/R_a$ isotopic ratios coincide with the results of Kis et al. (2019), reported for the emanations in the vicinity of the youngest Ciomadul volcano. In contrast to the Covasna gases, the Ciomadul gases are claimed to have (even if only partially) a magmatic origin (i.e., degassing of a presently situated lower crustal magmatic body may exist under the volcano; Kis et al., 2019). There are very similar $\delta^{13}C$ and $R_c/R_a$ isotopic ratios for Covasna and Ciomadul noble gases (later discussed in detail) even if the former location was associated with recently active volcanism and the latter was not. Kis et al. (2019) also acknowledged and discussed that deep, subduction related fluids may play role in the isotopic signatures found in the vicinity of the Ciomadul volcano. The authors considered mainly the role of magmatic sources in overprinting the original deep signature, but the impact of other crustal processes such as metamorphic products were excluded. Elevated mantle gas contributions in gases of springs and wells (compared to the atmosphere) in non-volcanic regions have been reported from several locations worldwide including the Vardar zone of Serbia (Randazzo et al., 2021), Central Italy (Rogie et al., 2000), Naxos Island (Cyclades, Greece; Siebenaller et al., 2013), Western Anatolia (Mutlu et al., 2008), Lower Engadine Valley in Switzerland (Bissig et al., 2006), San Andrea Fault (Kennedy and van Soest, 2007), and in the North China Craton (Chang et al., 2021). Besides the similarities in the $R_c/R_a$ values, all these localities have a similar geodynamic background (e.g., subduction) in terms of deep-seated deformation zones that support deep-seated fluid upflow (e.g., Pili et al., 2011; Précigout et al., 2019). In the shallow upper mantle, $CO_2$ is one of the most abundant fluid components (Tingle and Green, 1987) due to the similar inert behaviour as helium. By combining the $\delta^{13}C$ result of $CO_2$ with the helium isotopic ratio ($R_c/R_a$) on a $\delta^{13}C$ vs. $R_c/R_a$ diagram, we can determine the source region of both gases (Ciotoli et al., 2013). Our results fall onto the mantle-limestone mixing line (Fig. 5), even if the uncorrected helium isotopic ratios are used. This result assumes that, similar to helium, a subordinate amount of $CO_2$ originates from the Earth's mantle. This inference is also supported by the close similarity of the sampled $\delta^{13}C$ gases ($\delta^{13}C = -2.0$ to $-0.47$) with the upper mantle $\delta^{13}C$ isotopic ratio (−5.2; Marty and Zimmermann, 1999). Besides the helium and $CO_2$, we also discuss mantle $H_2O$ as the mantle source based on the

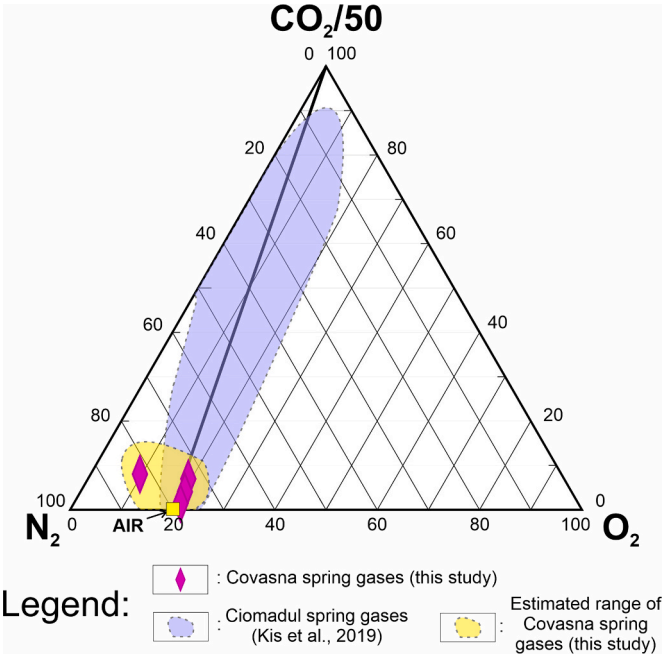


**Fig. 4.** The sampled gases presented on a $N_2$–$O_2$–$CO_2$/50 triplot compared with the southern Harghita Mountain emanating gases of Kis et al. (2019). The Covasna gases show high atmospheric contamination and therefore lie close to the 'AIR' end-member.

active sinking slab beneath the Southeastern Carpathians. However, $H_2O$, in contrast to helium and $CO_2$, is more likely to be incorporated into the solid upper mantle and can be found as a major component of hydrous minerals (e.g., amphibole, mica) or as trace (component as $H^+$) in nominally anhydrous minerals (e.g., olivine, pyroxenes) (e.g., Kovács et al., 2010; Demouchy and Bolfan-Casanova, 2016). The fingerprint of mantle $H_2O$, compared to $CO_2$ and helium has, therefore, a lower probability. Beneath the Southeastern Carpathians, mantle volatiles can originate at least from three different sources.

(1) One source of mantle volatiles is the rapidly sinking Vrancea slab, characterized by either subducted oceanic crust or delaminated thick continental lithospheric mantle (e.g., Mațenco et al., 2007; Ferrand and Manea, 2021; Petrescu et al., 2021; Kovács et al., 2021). The rapid sinking of the Vrancea slab can result in dehydration and decarbonation phase transformation reactions of high pressure and temperature phases (amphibole, e.g., Niida and Green, 1999; or mica, Bucher and Grapes, 2011 and references therein). These reactions will release fluids into the mantle wedge above at various depths based on the stability of the volatile-bearing phases (e.g., Manning, 2004). In the subducted oceanic slab, the dehydration of subducted serpentinite bodies can be one important source for $H_2O$ (Ferrand and Manea, 2021). Although structural and geochemical studies have questioned whether all serpentinite bodies of significant volumes could have formed and always transported to depths deeper than 100 km (Hermann and Lakey, 2021). In contrast, delamination of the continental lithosphere of the Moesian plate (Knapp et al., 2005; Petrescu et al., 2021; Borleanu et al., 2021) may well result in the decomposition of hydrous mantle minerals (e.g., amphibole, phlogopite) and carbonates. These minerals within the old

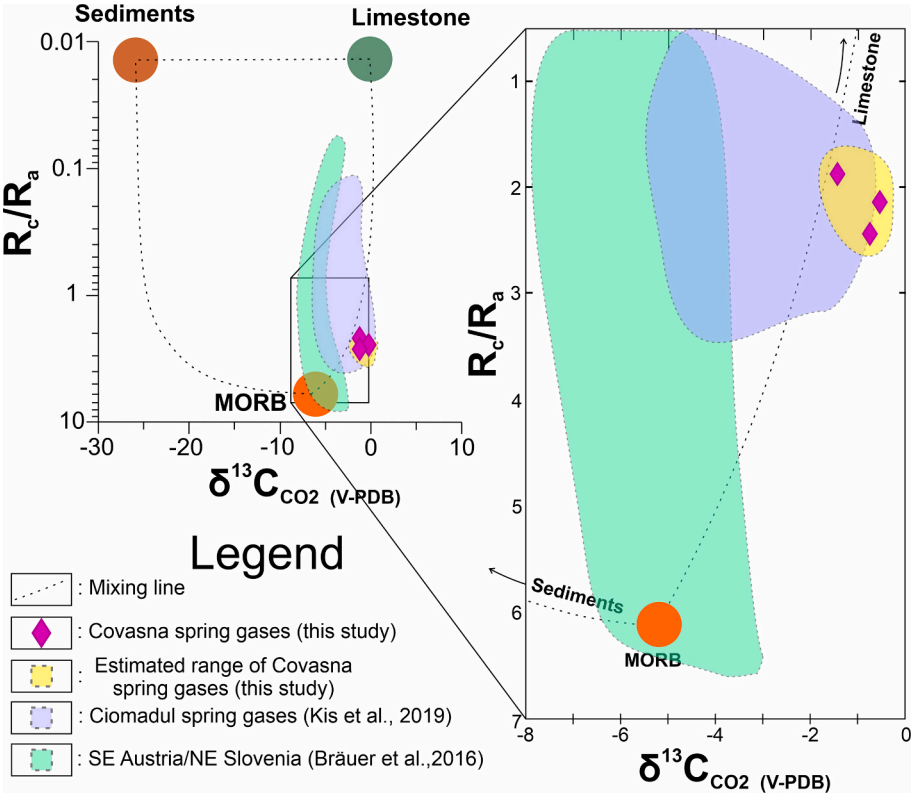


**Fig. 5.** $\delta^{13}C$ vs. $R_c/Ra$ (corrected $^3He/^4He$ ratio) stable isotope plot (Ciotoli et al., 2013) presenting dissolved gases in spring waters from Covasna. For comparison, we highlight the $\delta^{13}C$ and $R_c/Ra$ isotopic ratios of $CO_2$ and helium, respectively, from gas emanations in the Ciomadul area and springs (southern Harghita and Eastern Carpathians; Kis et al., 2019) and spring $CO_2$ gases from SE Austria/NE Slovenia (Bräuer et al., 2016). Our studied Covasna samples overlap with the Ciomadul $CO_2$ gases (Kis et al., 2019) and differ significantly from the SE Austria/NE Slovenia springs. MORB = Mid-ocean ridge basalt, V-PDB = Vienna Pee Dee Bee.

Precambrian basement and presumably continental lithospheric mantle can originate from metasomatic alteration occurring over long timescales (Griffin et al., 1999, 2009; Grégoire et al., 2003; Aulbach et al., 2017, 2020). The immediate increase in pressure and the delayed temperature increase in the subducted continental lithosphere (i.e., slab steepening and rapid sinking) destabilises the hydrous and carbonate phases and results in the release of $CO_2$- and $H_2O$-rich volatiles through subsolidus reactions or partial melting depending on changing P-T conditions (e.g., Green, 2015; Dasgupta, 2018).

(2) The second potential mantle source of $H_2O$- and $CO_2$-rich fluids in the Southeastern Carpathians is the asthenospheric upwelling located in the hinterland of the subducted slab (Russo et al., 2005; Martin et al., 2006; Ren et al., 2012; Popa et al., 2012; Kind et al., 2017). When compared with the first source, such a fluid carries an additional mantle signature as it is linked to presence of partial melt within the asthenosphere. In this view, the asthenosphere itself may be considered as a 'mega magma chamber'. The age of the Perșani Mts. basalts (1.2–0.6 Ma; Panaiotu et al., 2013; Seghedi et al., 2016) proves the recent material transport from the asthenosphere into the upper lithosphere (e.g., Faccini et al., 2020) and, thus, supporting the idea of a continuous, ongoing, asthenospheric fluid release. Cooling of a regional asthenospheric upwelling can also act as a source of mantle $CO_2$ that carries a mantle signature ($\delta^{13}C \sim -5.2$; $R/R_a = \sim 6.1$; Marty and Zimmermann, 1999; Gautheron and Moreira, 2002). This type of $CO_2$ differs from the metamorphic carbonate signature since its formation is a result of the continuous crystallization of the small amount of partial melt present in the asthenosphere (Berkesi et al., 2019; Kovács et al., 2021).

(3) The third potential source for fluids is the ambient lithospheric mantle, because in fluid inclusions of mantle xenoliths from the Perșani Mountain Volcanic Field significant amount of entrapped fluids were reported (Szabó et al., 2019; Lange et al., 2023). These fluid inclusions can have the potential to be mobilised during deformation.

#### 5.2.2. *Origin of the crustal signatures*

To constrain the crustal source for the emanating $CO_2$, we refer to the $\delta^{13}C$ vs. $R_c/R_a$ diagram (Fig. 5) to separate isotopic ratios derived from different crustal carbon-bearing source regions. As previously stated, our samples fall into the mantle-limestone mixing line (Fig. 5) and, thus, presume a dominantly carbonate-origin for the crustal $CO_2$ (Ciotoli et al., 2013). The Covasna data show a strong similarity with the data of Kis et al. (2019) obtained for the nearby southern Harghita Mountains' mineral waters (Fig. 5). We assume that the very similar evolution for the observed isotopic ratios can occur by crustal assimilation by deep fluids during fluid evolution (Ciomadul) and mixing of metamorphic and mantle fluid (Covasna). A significant deviation from the results of Bräuer et al. (2016) compared to the Ciomadul and Covasna data can be seen (Fig. 5). In case of the former a fast fluid upwelling from a mafic magma source (e.g., underplating) is assumed, where no or very small amount of crustal fluid addition occurs, consequently preserving the original mantle source in isotopic ratio. The more positive $\delta^{13}C$ isotopic rations of the Covasna gases ($\delta^{13}C = -2.0$ to $-0.47$‰) compared to the average mantle $\delta^{13}C$ isotopic ratio end member (−5.2‰; Marty and Zimmerman, 1999) shows a shift towards more positive ratios indicating that the $CO_2$ contribution derived from marine limestone, dolomite and/or calc-silicate sediments (e.g., carbonaceous siliciclasts). Such sediments can have significantly higher $\delta^{13}C$ isotopic ratios than those of mantle $CO_2$ (Sano and Marty, 1995). From these sediments, $CO_2$ is released through decomposition of carbonate minerals (i.e. decarbonation reaction) via, for example, fluid infiltration (e.g., Bissig et al., 2006). Beneath the Târgu Secuiesc Basin, Palaeozoic and Mesozoic marine sediments, containing carbonates, are interpreted as being located in upper crustal (shallower than 20 km) position to form the upper part of the Moesian platform (Merten et al., 2010). The thickness of calc-silicates (3–14 km; Tari et al., 1997; Merten et al., 2010) justifies them as a source for the abundant crustal $CO_2$. We assume that, similar to $CO_2$, the majority of the sampled $H_2O$ is also released from a crustal source through dehydration reactions, consequently, carrying a metamorphic signature as observed for the easter Covasna spring waters (Table 2, Fig. 3). Metamorphic decarbonation and dehydration reactions occur at elevated temperature and pressure (Marty and Zimmerman, 1999, Bucher and Grapes, 2011 and references therein). Our calculated depth-temperature curves (Fig. 6) for the Târgu Secuiesc Basin present low temperatures (400–450 °C) at the crust-mantle boundary, in agreement with the low heat flux of the Transylvanian Basin (Tiliță et al., 2018). Based on our calculated low temperatures and the stability field of the hydrous Ca-silicate minerals (e.g., Bucher and Grapes, 2011), we assume that it is very unlikely that fluid release in the crust occurred as a result of thermal breakdown.

Carbon-dioxide and $H_2O$ release in the middle and lower crust is triggered by changing the composition of the intergranular fluids (Bucher and Grapes, 2011). The reactions under isothermal and isobar conditions are controlled by the $X(CO_2)$ of the intergranular fluid primarily in a calc-silicate rocks (Bucher and Grapes, 2011 and references therein, Winter, 2014). Based on our temperature-depth curves, the present mid and lower crustal rocks (e.g., amphibolite, gneiss, assumed based on the study of Hauser et al., 2007) are presently found under greenschist – amphibolite facies conditions, precisely in a metastable state (Fig. 6/a). The $CO_2$-rich fluid input (from the mantle into the lower crust) results in phase transformation of the hydrous minerals and leads to carbonisation of the mid and lower crustal rocks (Winter, 2014). This suggests that significant amounts of crustal $H_2O$ can be released from the mid and lower crustal rocks. During the breakdown of hydrous minerals various alkaline and halogen elements are also released into the fluid (e.g., Na, K, Cl) (e.g., Niida and Green, 1999; Groppo et al., 2022) resulting in an $H_2O$–NaCl-(KCl)–$CO_2$ fluid system.

The upper crustal calc-silicate sediments of the Moesian platform (e.g., Tari et al., 1997; Merten et al., 2010) are situated in the prehnite-pumpellyite facies (Fig. 6/a). The lower positioned calc-silicate sediments (~15 km) are close to the prehnite-pumpellyite and greenschist facies boundary assuming metamorphic $H_2O$ release from hydrous minerals (Graham et al., 1983; Condit et al., 2020). This dehydration process is presumably the consequence of the thin-skinned nappe stacking (11-8 Ma, Matenco, 2017; Ismail-Zadeh et al., 2012 and references therein) that lead to the burial of the Moesian platform sediments.

Likewise to the mid and lower crustal rocks, fluids in the upper crust can be released through fluid infiltration. Based on the mineral breakdown in the lower and mid crust, the composition of the penetrating fluid can be primarily described as a $H_2O$–NaCl–$CO_2$ system (Manning et al., 2013). A possible case for upper crustal $CO_2$ release is when an $H_2O$–$CO_2$–NaCl fluid enters the carbonate sediments in the upper crust leading to carbonate dissolution, consequently releasing $CO_2$ (Manning et al., 2013). The thickness of the Mesozoic-Paleozoic calc-silicates (carbonates, carbonaceous siliciclasts) beneath the Târgu Secuiesc Basin (5–18 km; Merten et al., 2010) makes these sediments a proper source for crustal $CO_2$. Another virtual source for crustal $CO_2$ is the uppermost flysch sediments as they contain high amounts of carbonate minerals (Roban et al., 2020). Compared to the Mesozoic-Palaeozoic carbonaceous sediments, the flysch can also contain high amounts of graphite and organic carbon compounds (e.g., hydrocarbon) (Roban et al., 2020). The release of $CO_2$ from these carbon-bearing compounds would cause the shift of $\delta^{13}C$ towards more negative values (Fig. 5) and, therefore, hinders the possibility to be the source of crustal $CO_2$. Finally, the groundwater can carry $CO_2$ from the atmosphere into the underground water system and with time dissolve further $CO_2$. Based on the cold-water temperature of the gas-rich springs, the groundwater only reached shallow levels (presumably few 100 m) and did not have enough time to dissolve high amounts of $CO_2$ (Barros et al., 2021).

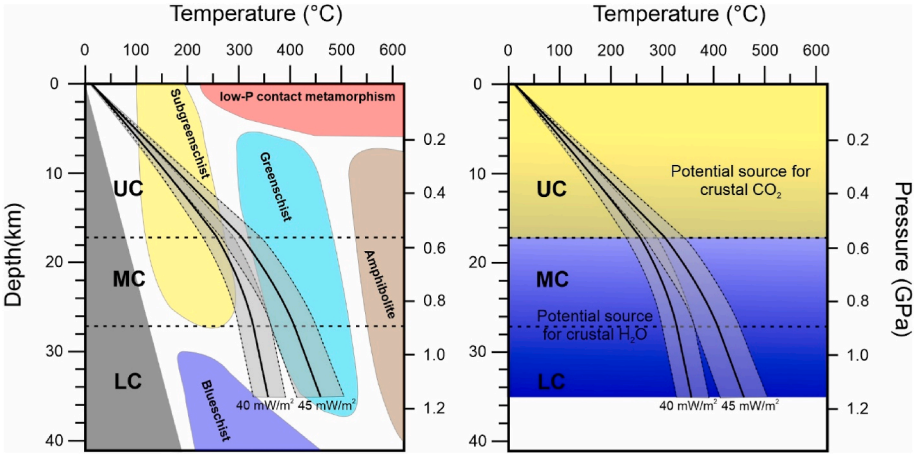


**Fig. 6.** (a) Calculated temperature-depth curves for 40 and 45 W/m$^2$ for the Târgu Secuiesc Basin together with the (a) metamorphic facies provinces (Bucher and Grapes, 2011) and (b) the most likely source regions for the crustal $CO_2$ (yellow) and $H_2O$ (blue). Crustal layers are based on Hauser et al. (2007). The calculated temperature of the MOHO lies between 350 and 450 °C and corresponds to the upper greenschist facies conditions. UC: Upper crust, MC: Middle crust, LC: Lower crust. (For interpretation of the references to colour in this figure legend, the reader is referred to the Web version of this article.)

Altogether, taking into account all the above considerations, the most suitable source region for the release of crustal $CO_2$ is the lower part of the upper crust (Fig. 6/b).

The low $^4He/^{20}Ne$ values of the sampled gases (Table 4, Fig. 7) indicate that the sampled gases are rich in atmospheric component, also supported by the week correlation between the $R_c/R_a$ and dissolved $N_2$ concentration (Table 4). Several processes can increase the atmospheric signal. First, when deep fluids mix with shallow subsurface groundwaters (Etheridge et al., 1983) carrying atmospheric noble gas isotope signals (e.g., Méjean et al., 2020). Second, when deep mixing (>3 km) occurs between deep-origin fluids and atmospheric gas-saturated subsurface waters (Méjean et al., 2020). A third scenario is that the mantle/lower crust source regions had initially a low $^4He/^{20}Ne$ ratio (Barry et al., 2015) and, thus, no interaction between subsurface waters of different origins is needed. The high crustal contribution of Covasna gases (e.g., based on the $\delta^{13}C$ results) contradicts a potential low $^4He/^{20}Ne$ ratio of the source region because the crust is associated with a high $^4He$ value due to the alpha decay of U and Th (Sano and Marty, 1995). The deep mixing of the fluids is inconsistent with the low temperature of the gas-rich springs. Consequently, a shallow groundwater level mixing is assumed. This is supported by the $\delta^2H$ and $\delta^{18}O$ mixing line between the local meteoric water line and the metamorphic $H_2O$ (Fig. 3) together with the relevant spatial distribution of the mixing ratio (i.e., from the centre of the Târgu Secuiesc Basin towards its margin).

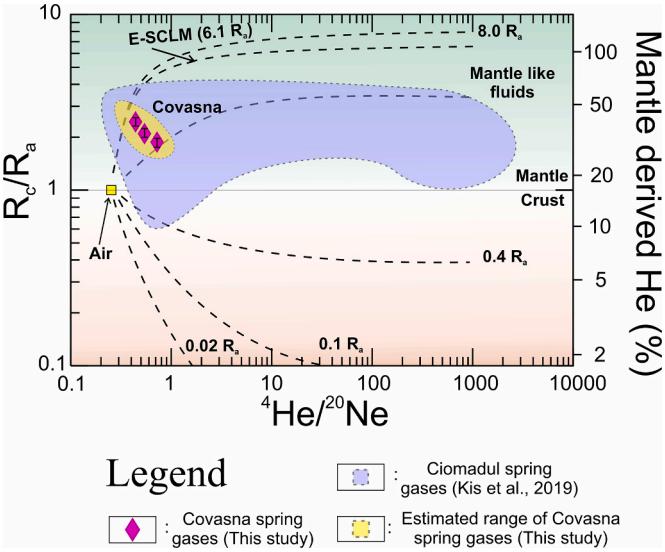


**Fig. 7.** $R_c/R_a$ (corrected $^3He/^4He$ ratio) vs. $^4He/^{20}Ne$ diagram (modified after Sano and Wakita (1985)) with values of the Covasna spring gases in comparison with same isotopic ratios of Kis et al. (2019) from the southern Harghita Mountains. Black lines on the Covasna samples present the sample error. The Covasna gases show high similarity with the southern Harghita Mountains. Dashed lines represent different mixing lines between the mantle ($R/R_a = 8.0$; $^4He/^{20}Ne = 1000$), crust ($R/R_a = 0.02$, $^4He/^{20}Ne = 1000$) and atmosphere. In case of the atmospheric end-member the $R/R_a$ and $^4He/^{20}Ne$ isotopic ratios correspond to the dissolved air in 5 °C spring waters ($R/R_a = 1$, $^4He/^{20}Ne = 0.274$). Mantle like fluid line was taken from Kis et al. (2019). The line of E-SCLM (European Subcontinental Lithospheric Mantle; $R/R_a = 6.1 \pm 0.9$, $^4He/^{20}Ne = 1000$) was taken from Gautheron and Moreira (2002).

### 5.2.3. *Evolution of the deep-source fluids in the Târgu Secuiesc Basin*

The previous discussion envisages multiple sources for the Târgu Secuiesc Basin deep-origin fluids. The inherited deep signal (based on the $R_c/R_a$ results) assumes fast fluid upwelling linked to the high tectonic deformation rates and vertical differential movements (Sleep and Blanpied, 1992; Mațenco, 2017). Deep-seated deformation zones within the Moesian platform formed during the late-stage thick-skinned thrusting that took place in the Southeastern Carpathians (Merten et al., 2010), which can increase fluid flux (Etheridge et al., 1983). These weakening zones are interpreted to continue down to the crust-mantle boundary, but whether they continue further down into the lithospheric mantle is an open question (Fig. 8). The presence of mylonite and ultramylonite textured upper mantle ultramafic xenoliths (Falus et al., 2008, 2011) from the nearby Perșani Mountain Volcanic Field strongly suggests that the deep-seated weakening zones are likely to continue into the lithospheric mantle and enhance mantle fluid flux as discussed below (Précigout et al., 2019). Therefore, the presence of lithospheric scale weakening zones in the Southeastern Carpathians provide a good mantle-to-surface connection, and thus supports a continuous fluid flow from the deep lithosphere to the surface.

An overview of the deep fluid evolution beneath the Southeastern Carpathians is presented in Fig. 8/a. Mantle volatile-rich fluids may have various compositions (i.e., their $CO_2/H_2O$ molar ratio or $X(CO_2)$) based on their source region. At ambient mantle conditions, the volatile-rich fluids are dominantly $CO_2$- and $H_2O$-rich (>95 mol%, Green, 2015). This type of fluids can form a complete fluid miscibility with each other and with other volatile fluid components (e.g., noble gases, dissolved alkalis, e.g., Manning et al., 2013) and can also dissolve low amounts of silicate melt components (Sterner and Bodnar, 1991; Newton and Manning, 2008). Fluids from an asthenospheric source and from the

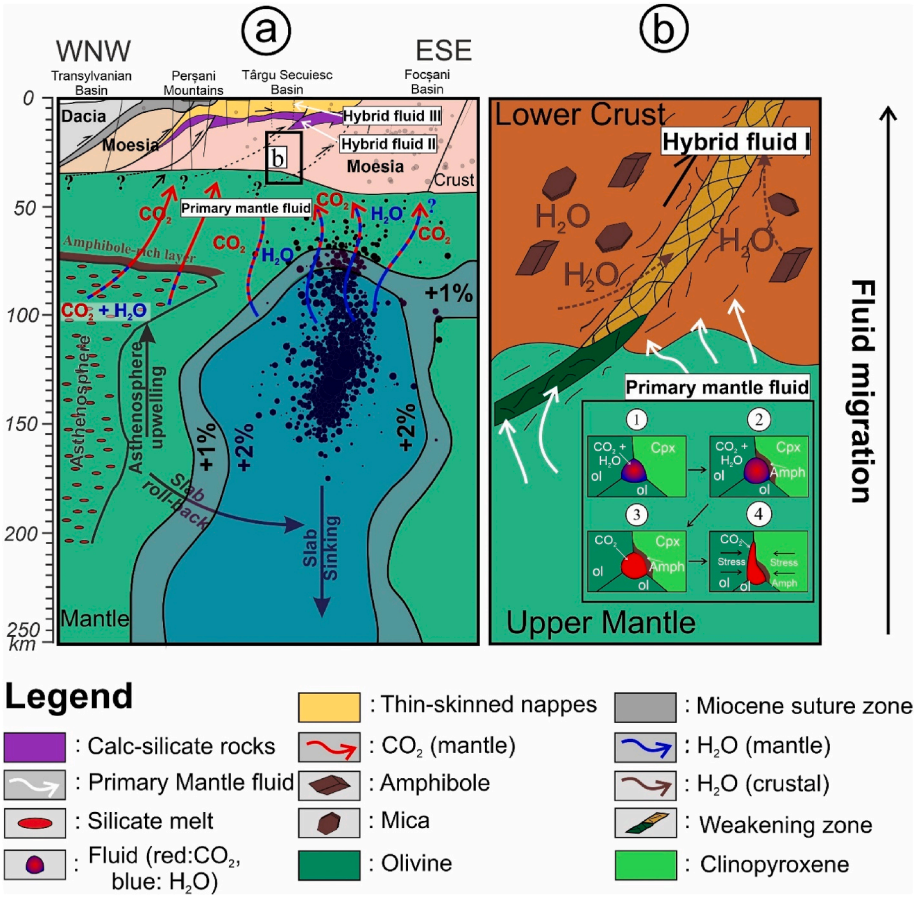


**Fig. 8.** Cartoon showing the fluid evolution in the tectonic regime of the SE Carpathians. a: WNW-ESE cross section illustrating the fluid migration path from the upper mantle sources towards the lower crust (modified from Mațenco et al., 2007; Tiliță et al., 2018). The amphibole-rich layer is assumed based on Kovács et al. (2021). The 1–2% values around the sinking slab relate to the increase in seismic attenuation (Mațenco et al., 2007); b: fluid evolution near the boundary between the upper mantle and lower crust. The question mark relates to position and the continuity of the deep-seated deformation zones. The small figures (1-4) in b present the evolution of intergrain fluid. b/1 The $CO_2$–$H_2O$ fluid gets trapped at grain triple junctions where (b/2) continuous amphibole crystallization takes place (b/3) relativly enriching the fluid in $CO_2$. Due to the intensive stress in the active geodynamic region, the fluid eventually gets squeezed out and migrates towards the surface (b/4). Cpx = Clinopyroxene, Amph = Amphibole.

sinking Vrancea slab have a lower $CO_2/H_2O$ molar ratio compared to the lithospheric mantle, which will increase when these fluids reach the shallow lithospheric mantle region. In case of an asthenospheric fluid, this increase is owed presumably to amphibole formation at the lithosphere-asthenosphere boundary (Green et al., 2010; Kovács et al., 2021), whereas fluids from the sinking slab will mix with the increased $CO_2/H_2O$ molar ratio fluids of the shallower lithospheric fluids. The strongly deformed lithospheric mantle will enhance fluid migration due to the $CO_2$ incompatibility with silicate minerals (Shcheka et al., 2006), and will migrate along grain boundaries to the crust-mantle boundary (‘*Primary mantle fluid*’; Fig. 8/b). Additionally, the deep-seated weakening zones also support mantle-derived fluid (‘*Primary mantle fluid*’) migration from the upper lithospheric mantle into the lower crust (Fig. 8/b). This is owed to the increased grain surface-to-volume ratio within the deformation zones compared to the neighbouring (undeformed or less deformed) zone accompanied with grain misfit structures (Précigout et al., 2019). The inflow of the mantle-derived $CO_2$-rich fluids into the lower crust will consequently increase $CO_2$ molar ratio of the lower crustal pore fluid and, therefore, initiate devolatilization metamorphic reactions of hydrous minerals (e.g., amphibole, mica) releasing metamorphic $H_2O$-rich fluid (Newton, 1986; Winter, 2014). The dehydration metamorphic reactions will consume significant amount of mantle $CO_2$ and result in the formation of carbonate minerals (Winter, 2014) within the lower crust. The released metamorphic $H_2O$-rich fluid will have a high salinity due to the simultaneous release of alkalis (e.g., Na, K) and halogens (e.g., Cl) and mix with the mantle-derived fluids forming a new ‘*hybrid fluid (I)*’. The newly formed fluid will migrate further upwards along deep-seated deformation zones. In this stage of fluid evolution the ‘*hybrid fluid (I)*’ will dominantly represent a $H_2O$–Na(K)Cl–$CO_2$ system. The migration of the fluid in a ductile lower crustal regime is modelled by Sleep and Blanpied (1992), who proposed that a cycle of stress, earthquake/nappe movement and fluid migration occurs in the ductile lower crust supporting episodic fluid flow. The recent rapid evolution of the Southeastern Carpathians area assumes such a rapid cyclicity and could explain how fast fluid supply is provided from the lower crust into the upper-level carbonate bearing sediments. Furthermore, the frequent high magnitude mantle and crustal earthquakes initiated in the vicinity of the sinking Vrancea slab (Popescu et al., 2017; Ferrand and Manea, 2021) further destabilize the environment and increases the grain surface misfit within the weakening zones.

Multiple reactions can occur for the ‘*hybrid fluid (I)*’ after reaching the upper crustal carbonate-bearing sediments (including sediments of the thin-skinned nappes). The inter-grain $H_2O$-rich fluid of the upper crustal carbonate-bearing sediments will shift the penetrating $H_2O$–Na(K)Cl–$CO_2$ fluid towards a higher $H_2O$ molar ratio resulting into ‘*hybrid fluid (II)*’. The enrichment of $H_2O$ will provide the opportunity for carbonate dissolution (Manning et al., 2013), therefore, supporting the release of crustal $CO_2$. The $CO_2$ release will shift the residual mantle $\delta^{13}C$ isotopic ratio of the $CO_2$ fluid towards a more positive crustal $\delta^{13}C$ ratio

value. In addition, when $CO_2$ dissolves as [$CO_3$] in the '*hybrid fluid (II)*' it will interact with Na and form Na-bicarbonate complex (Manning et al., 2013). The facies of the water will therefore be a Na-bicarbonate type water with high $CO_2$ content as determined for the Covasna spring waters (Vaselli et al., 2002; Cseresznyés et al., under review) and the surrounding region (Kis et al., 2020).

The *hybrid fluid (II)*' will eventually migrate towards the surface from the crystalline basement along weakening zones such as the thin-skinned nappe boundaries. Faults, like those found at the Târgu Secuiesc Basin margin, will further drive the fluid until it reaches the surface (Etheridge et al., 1983). Part of the fluids can mix near the surface with groundwater overprinting the $\delta^2H$ and $\delta^{18}O$ stable isotope values of $H_2O$ leading to the formation of '*hybrid fluid (III)*'. In summary, the fluid evolution in the Southeastern Carpathians is likely the result of the multistage tectonic and geological evolution of the collisional orogen.

#### 5.2.4. *Volcanic versus deep-origin during 'post magmatic' activity*

In geodynamically active areas, simultaneous magmatic and non-magmatic (e.g., metamorphic) $CO_2$ emanation can occur as it is assumed in the Southeastern Carpathians (Vaselli et al., 2002; Kis et al., 2019). The latest eruption in the Eastern Carpathians was the Ciomadul volcano (last erupted ~ 28 ka; Karátson et al., 2019) that is ca. 50 km apart from the Târgu Secuiesc Basin. The emanating gases of the presumed Ciomadul magma chamber (Harangi et al., 2015; Laumonier et al., 2019) are described as a post-magmatic phenomenon and show similar $\delta^{13}C$ and $R_c/R_a$ isotopic ratios with the south-eastern Târgu Secuiesc gases (Fig. 5). Between the two regions numerous steep faults are found (Fielitz and Seghedi, 2005) and, therefore, it is unlikely that a direct fluid pathway connection exists between the two regions. Our study highlights that the similarity in the isotopic ratios in the two nearby areas (Fig. 5) is owed to the similar fluid evolution that can occur during magma evolution (e.g., crustal assimilation, fractionation) and spontaneous mantle degassing (i.e., primary mantle fluid went through crustal isotopic change). In addition, reverse contamination of the more evolved fluid can occur in the case of deep, residual fluid reservoirs or magma chambers through mantle fluid infiltration via deep-seated deformation zones (e.g., Fielitz and Seghedi, 2005). Such deep-seated deformation zones control magma transport (Fielitz and Seghedi, 2005) and, consequently, also mantle fluids migration. Mantle fluid isotopic change and evolution can be also equally assumed in the case of the (deep) crustal fluid storage systems beneath Ciomadul volcano, providing an alternative explanation besides the preferred degassing magma chamber scenario (Kis et al., 2019; Molnár et al., 2018). This would suggest that mantle fluid continuously resupplies the deep crustal fluid storage systems while preserving features of the former fluid storage systems that can be observed via geophysical methods (Popa et al., 2012; Harangi et al., 2015). The degree of crustal fingerprint of the new upwelling mantle fluids remains an open question as the deep crustal fluid storage systems gets continuously overprinted by crustal fluids or newly released fluids via mineral phase transformations (e.g., decarbonation and devolatilization reactions) (Althaus et al., 2000; Vaselli et al., 2002). Nevertheless, our case study in the Târgu Secuiesc Basin shows that fluid emanations in the so called mofette aureola of the East Carpathian's volcanic range (e.g., Airinei and Pricăjan, 1975; Vaselli et al., 2002; Kis et al., 2020) is complex as it includes multiple sources (the upper mantle, the lower crust and occasionally upper crustal sedimentary sequences) and active deformation zones and may not necessarily linked to active volcanism.

### 5.3. *A global outlook on deeply rooted $CO_2$-rich surface fluid emanations*

Knowledge on the lithospheric mantle beneath the Southeastern Carpathians and on the surface-emerging volatiles in the southeastern part of the Târgu Secuiesc Basin defines the deep and surface chemical end-members, respectively (e.g., Falus et al., 2000, 2008; Italiano et al., 2017; Kis et al., 2020). Similar mantle-to-surface relationships through lithospheric deformation zones have been proposed for fluid emanations in various tectonic settings globally (e.g., Bissig et al., 2006; Kennedy and van Soest, 2007; Mutlu et al., 2008; Pili et al., 2011; Barros et al., 2021; Chang et al., 2021; Zhang et al., 2021). The firstly observed similarity of the above listed regions with the Târgu Secuiesc Basin is the strong spatial relationship of the deep-origin signals of the fluid emanations and deep-seated deformation zones. Furthermore, deep-seated and steeper deformation zones may provide faster fluid migration paths, hence, mantle derived fluid signals could be better detected (e.g., Bräuer et al., 2016; Vauchez et al., 2012; Randazzo et al., 2021). Nevertheless, regardless of the tectonic setting, the migration of the fluids is always controlled by the deep-seated deformation zones whether they are released by higher temperature reactions (e.g., the formation of wollastonite above 600 °C; Bucher and Grapes, 2011) or fluid-induced decarbonation (e.g., Kerrick and Caldeira, 1998). Studies in several regions explain the importance of $H_2O$-rich fluids in the release of crustal $CO_2$ (e.g., Kerrick and Caldeira, 1998; Barros et al., 2021) and show, again, a similar behaviour with the Târgu Secuiesc Basin.

The existence of mylonitic mantle xenoliths from the Perșani Mountains Volcanic Field in the close vicinity of the Târgu Secuiesc Basin (Falus et al., 2008, 2011) gives an excellent insight into the upper mantle and probably lower crustal deformations (Vauchez et al., 2012). These deformation signs support continuation of deformation zones from the ductile upper mantle and lower crust into brittle, fault-dominated upper crust (Vauchez et al., 2012). This connection may explain the fast fluid upwelling leading to stronger mantle fluid signatures in the gas-rich springs of the Southeastern Carpathians, San Andreas Fault (Kennedy and van Soest, 2007) and the eastern Alps (Bräuer et al., 2016). Additionally, multiple deep-seated deformation zones can increase mantle volumes affected by deformation and also increase the amount of released fluids from the upper mantle (Vauchez et al., 2012). Reactivation of shear zones in the upper crust (above the brittle-ductile deformation boundary) along the deep-seated deformation zones can be traced by seismicity and can be triggered by the accumulated fluid pressure (e.g., Lemonnier et al., 1999). The presence of these weakening zones further support fluid mobility even when the deformation events cease or weaken (Chang et al., 2021). Therefore, constant $CO_2$ emanation can postdate the deformation event itself (Chang et al., 2021), especially when reactivation of the faults and ductile deformation zones in the upper crust and lower lithosphere, respectively, occurs (e.g., Sleep and Blanpied, 1992). As frequent intermediate-depth earthquakes are observed in the deep-seated deformation-bearing areas (e.g., Himalayas, Lemonnier et al., 1999) it is reasonable to assume that variations in the surface gas emanations prior to larger earthquakes could act as earthquake precursors (Szakács, 2021; Kovács et al., 2021).

## 6. Conclusions

Carbon-dioxide-rich mineral waters and their dissolved gases have a combined metamorphic and presumably mantle origin in the Târgu Secuiesc Basin. These signatures are related to the fast fluid upwelling and high deformation rate that characterise the recent geodynamic evolution of the Southeastern Carpathians.

The $CO_2$-rich fluids show complex multistage origin including processes from the upper mantle to the surface. In a succession of steps, each of them contributing to the changes of the chemical and isotopic signatures of the surface-emerging fluids. The primary inflow of presumably $CO_2$-rich fluids into the lower crust results in dehydration metamorphic reactions, during which the majority of the mantle $CO_2$ is consumed. The newly released metamorphic $H_2O$ (+ alkalis and halogens) and residual mantle $CO_2$ migrate to the upper crust penetrating carbonate bearing sedimentary crustal rocks. As a result of fluid-solid interaction carbonate minerals get dissolved enriching the fluid in

crustal carbonate component. The most important crustal carbon source may be the calc-silicates (carbonates, calcareous siliciclasts) found in the upper Moesian platform, but the presence of the carbonates-bearing flysch sediments cannot be ruled out. Additionally, when $CO_2$ is dissolved as $[CO_3^{2-}]$, it interacts with Na forming Na-bicarbonate complexes that will eventually define the gas-rich spring water facies of the Târgu Secuiesc Basin.

Finally, the deep fluid signature (i.e., elevated $R_c/R_a$ ratio and metamorphic $H_2O$) is strongly controlled by the position of the gas-rich spring with respect to the faults of the Târgu Secuiesc Basin margin. The isotopic overprint by deep fluid mixing with the shallow underground water is weakened in the vicinity of the faults and elevated topography, whereas it is strengthened towards the basin where faults are absent on a lower topography.

Our results highlight the importance of deep upper mantle fluids in the generation of surface $CO_2$-rich emanations and reveal the importance of interconnection between upper mantle and lower crustal ductile deformation zones and upper crustal faults. Carbon dioxide-rich surface emanations are not necessarily related to active volcanic or post-volcanic activities but can also be present in tectonic settings with active lithospheric scale deformations without any surface manifestation of contemporaneous volcanism or post volcanic activity. These focused or more diffuse $CO_2$-rich emanations in actively deforming areas must also be considered when the global quantitative $CO_2$ emission is estimated.

## Declaration of competing interest

The authors declare that to their knowledge they have no known competing financial interests or personal relationships that could have influence the results and conclusions reported in this paper.

## Data availability

Data will be made available on request.

## Acknowledgements

This study was financially supported by the MTA FI Lendület Pannon Lit$H_2$Oscope Research Group, the NKFIH K141956 Topo-Transylvania grant, and ELKH infrastructural support. Thomas Lange was financially supported from the ÚNKP-21-3-II-ELTE-846 New National Excellence Program of the Ministry for Innovation and Technology. This is the 112. publication of the Lithosphere Fluid Research Lab (LRG).

## Appendix A. Supplementary data

Supplementary data to this article can be found online at https://doi.org/10.1016/j.eve.2023.100013.

## References

Airinei, Ş., Pricăjan, A., 1975. Some geological connections between the mineral carbonic and thermal waters and the post-vulcanic manifestations correlated with the deep geological structure of the East Carpathians territory–Romania. Institutul de Geologie și Geofizică, Studii Tehnice și Economice, Seria E, Hidrogeologie (12).
Althaus, T., Niedermann, S., Erzinger, J., 2000. Noble gas studies of fluids and gas exhalations in the East Carpathians, Romania. Chem. Erde-Geochem. (60),, 189–207.
Andreescu, M., Demetrescu, C., 2001. Rheological implications of the thermal structure of the lithosphere in the convergence zone of the Eastern Carpathians. J. Geodyn. 31 (4), 373–391.
Andreescu, M., Nielsen, S.B., Polonic, G., Demetrescu, C., 2002. Thermal budget of the Transylvanian lithosphere. Reasons for a low surface heat-flux anomaly in a Neogene intra-Carpathian basin. Geophys. J. Int. 150, 494–505.
Aulbach, S., Massuyeau, M., Gaillard, F., 2017. Origins of cratonic mantle discontinuities: a view from petrology, geochemistry and thermodynamic models. Lithos 268, 364–382.
Aulbach, S., Massuyeau, M., Garber, J.M., Gerdes, A., Heaman, L.M., Viljoen, K.S., 2020. Ultramafic carbonated melt-and auto-metasomatism in mantle eclogites: compositional effects and geophysical consequences. Geochem. Geophys. Geosys. 21 (5), e2019GC008774.
Bădescu, D., 2005. Evoluţia Tectono-Stratigrafică a Carpaţilor Orientali În Decursul Mezozoicului Şi Neozoicului. Editura Economică (In Romanian).
Bandrabur, T., 1962. Cercetari higrogeologie in regiunea Covasna-Tufalau-Peteni. Dari de Seama ale Sedintelor XLIX (1961–1962), 193–211.
Bandrabur, T., 1967. Observatiuni geologice si hidrogeologice in zona Tg. Secuiesc. Studii de Hidrogeologie 87–102.
Barros, R., Defourny, A., Dassargues, A., Piessens, K., Welkenhuysen, K., 2021. A review of the geology and origin of CO2 in mineral water springs in east Belgium. Geol. Belg. 24 (1–2).
Barry, P.H., Hilton, D.R., Day, J.M., Pernet-Fisher, J.F., Howarth, G.H., Magna, T., Agashev, A.M., Pokhilenko, N.P., Pokhilenko, L.L., Taylor, L.A., 2015. Helium isotopic evidence for modification of the cratonic lithosphere during the Permo-Triassic Siberian flood basalt event. Lithos 216, 73–80.
Bense, V.F., Gleeson, T., Loveless, S.E., Bour, O., Scibek, J., 2013. Fault zone hydrogeology. Earth Sci. Rev. 127, 171–192.
Berkesi, M., Czuppon, G., Szabó, C., Kovacs, I., Ferrero, S., Boiron, M.C., Peiffert, C., 2019. Pargasite in fluid inclusions of mantle xenoliths from northeast Australia (Mt. Quincan): evidence of interaction with asthenospheric fluid. Chem. Geol. 508, 182–196.
Bissig, P., Goldscheider, N., Mayoraz, J., Surbeck, H., Vuataz, F.D., 2006. Carbogaseous spring waters, coldwater geysers and dry CO2 exhalations in the tectonic window of the Lower Engadine Valley, Switzerland. Eclogae Geol. Helv. 99 (2), 143–155.
Borleanu, F., Petrescu, L., Enescu, B., Popa, M., Radulian, M., 2021. The missing craton edge: crustal structure of the East European Craton beneath the Carpathian Orogen revealed by double-difference tomography. Global Planet. Change 197, 103390.
Bräuer, K., Kämpf, H., Strauch, G., 2014. Seismically triggered anomalies in the isotope signatures of mantle-derived gases detected at degassing sites along two neighboring faults in NW Bohemia, central Europe. J. Geophys. Res. Solid Earth 119 (7), 5613–5632.
Bräuer, K., Geissler, W.H., Kämpf, H., Niedermannn, S., Rman, N., 2016. Helium and carbon isotope signatures of gas exhalations in the westernmost part of the Pannonian Basin (SE Austria/NE Slovenia): evidence for active lithospheric mantle degassing. Chem. Geol. 422, 60–70.
Bucher, K., Grapes, R., 2011. Petrogenesis of Metamorphic Rocks. Springer Science & Business Media.
Bucher, K., Grapes, R., 2011. Petrogenesis of Metamorphic Rocks. Springer Science & Business Media.
Buttitta, D., Capasso, G., Paternoster, M., Barberio, M.D., Gori, F., Petitta, M., Picozzi, M., Caracausi, A., 2023. Regulation of deep carbon degassing by gas-rock-water interactions in a seismic region of Southern Italy. Sci. Total Environ. 897, 165367.
Caracausi, A., Sulli, A., 2019. Outgassing of mantle volatiles in compressional tectonic regime away from volcanism: the role of continental delamination. Geochem. Geophys. Geosys. 20 (4), 2007–2020.
Cermák, V., 1993. Lithospheric thermal regimes in Europe. Phys. Earth Planet. Inter. 79, 179–193.
Chaillou, G., Couturier, M., Tommi-Morin, G., Rao, A.M., 2014. Total alkalinity and dissolved inorganic carbon production in groundwaters discharging through a sandy beach. Procedia Earth Planet. Sci. 10, 88–99.
Chang, L., Ying, L., Zhi, C., Zhaofei, L., Yuanxin, Z., Le, H., 2021. Fluid Geochemistry within the North China Craton: Spatial Variation and Genesis. Geofluids, 2021.
Chapman, D.S., Furlong, K.P., 1992. Thermal state of the continental crust. In: Fountain, D.M., Arculus, R., Kay, R.W. (Eds.), Continental Lower Crust. Elsevier, Amsterdam, pp. 179–199.
Chiodini, G., Cardellini, C., Amato, A., Boschi, E., Caliro, S., Frondini, F., Ventura, G., 2004. Carbon dioxide Earth degassing and seismogenesis in central and southern Italy. Geophys. Res. Lett. 31 (7).
Ciotoli, G., Etiope, G., Florindo, F., Marra, F., Ruggiero, L., Sauer, P.E., 2013. Sudden deep gas eruption nearby Rome's airport of Fiumicino. Geophys. Res. Lett. 40 (21), 5632–5636.
Ciulavu, D., Dinu, C., Szakács, A., Dordea, D., 2000. Neogene kinematics of the Transylvanian basin (Romania). AAPG Bull. 84 (10), 1589–1615.
Condit, C.B., Guevara, V.E., Delph, J.R., French, M.E., 2020. Slab dehydration in warm subduction zones at depths of episodic slip and tremor. Earth Planet Sci. Lett. 552, 116601.
Cseresznyés, D., Király, Cs., Gál, Á., Papucs, A., Kónya, P., Lakos, I., Rinyu, L., Szamosfalvi, Á., Szabó, Cs., Falus, Gy., Czuppon, Gy. (under review) Surface occurrence of dawsonite and natural CO2 emanation in Covasna, in the Eastern Carpathians: a stable isotope study. Chemical Geology, CHEMGE15674, under review.
Dasgupta, R., 2018. Volatile-bearing partial melts beneath oceans and continents–where, how much, and of what compositions? Am. J. Sci. 318 (1), 141–165.
Demetrescu, C., Veliciu, S., 1991. Heat flow and lithosphere structure in Romania. Terrestrial Heat Flow and the Lithosphere Structure 187–205.
Demouchy, S., Bolfan-Casanova, N., 2016. Distribution and transport of hydrogen in the lithospheric mantle: a review. Lithos 240, 402–425.
Downes, H., Seghedi, I., Szakacs, A., Dobosi, G., James, D.E., Vaselli, O., Rigby, I.J., Ingram, G.A., Red, D., Pécskay, Z., 1995. Petrology and geochemistry of late Tertiary/Quaternary mafic alkaline volcanism in Romania. Lithos 35 (1–2), 65–81.
Etheridge, M.A., Wall, V.J., Vernon, R.H., 1983. The role of the fluid phase during regional metamorphism and deformation. J. Metamorph. Geol. 1 (3), 205–226.
Evans, M.J., Derry, L.A., France-Lanord, C., 2008. Degassing of metamorphic carbon dioxide from the Nepal Himalaya. Geochem., Geophys., Geosyst. 9 (4).
Faccini, B., Rizzo, A.L., Bonadiman, C., Ntaflos, T., Seghedi, I., Grégoire, M., Ferretti, G., Coltorti, M., 2020. Subduction-related melt refertilisation and alkaline

metasomatism in the Eastern Transylvanian Basin lithospheric mantle: evidence from mineral chemistry and noble gases in fluid inclusions. Lithos 364, 105516.
Falus, G., Szabó, C., Vaselli, O., 2000. Mantle upwelling within the Pannonian Basin: evidence from xenolith lithology and mineral chemistry. Terra. Nova 12 (6), 295–302.
Falus, G., Tommasi, A., Ingrin, J., Szabó, C., 2008. Deformation and seismic anisotropy of the lithospheric mantle in the southeastern Carpathians inferred from the study of mantle xenoliths. Earth Planet Sci. Lett. 272 (1–2), 50–64.
Falus, G., Tommasi, A., Soustelle, V., 2011. The effect of dynamic recrystallization on olivine crystal preferred orientations in mantle xenoliths deformed under varied stress conditions. J. Struct. Geol. 33 (11), 1528–1540.
Ferrand, T.P., Manea, E.F., 2021. Dehydration-induced earthquakes identified in a subducted oceanic slab beneath Vrancea, Romania. Sci. Rep. 11 (1), 1–9.
Fielitz, W., Seghedi, I., 2005. Late Miocene–Quaternary volcanism, tectonics and drainage system evolution in the East Carpathians, Romania. Tectonophysics 410 (1–4), 111–136.
Frezzotti, M.L., Touret, J.L., 2014. CO2, carbonate-rich melts, and brines in the mantle. Geosci. Front. 5 (5), 697–710.
Gautheron, C., Moreira, M., 2002. Helium signature of the subcontinental lithospheric mantle. Earth Planet Sci. Lett. 199 (1–2), 39–47.
Giggenbach, W.F., Sano, Y., Wakita, H., 1993. Isotopic composition of helium, and CO2 and CH4 contents in gases produced along the New Zealand part of a convergent plate boundary. Geochem. Cosmochim. Acta 57 (14), 3427–3455.
Girbacea, R., Frisch, W., 1998. Slab in the wrong place: lower lithospheric mantle delamination in the last stage of the Eastern Carpathian subduction retreat. Geology 26 (7), 611–614.
Göğüş, O.H., Pysklywec, R.N., Faccenna, C., 2016. Postcollisional lithospheric evolution of the Southeast Carpathians: comparison of geodynamical models and observations. Tectonics 35 (5), 1205–1224.
Graham, C.M., Greig, K.M., Sheppard, S.M.F., Turi, B., 1983. Genesis and mobility of the $H_2O$-$CO_2$ fluid phase during regional greenschist and epidote amphibolite facies metamorphism: a petrological and stable isotope study in the Scottish Dalradian. J. Geol. Soc. 140 (4), 577–599.
Green, D.H., 2015. Experimental petrology of peridotites, including effects of water and carbon on melting in the Earth's upper mantle. Phys. Chem. Miner. 42 (2), 95–122.
Green, D.H., Hibberson, W.O., Kovács, I., Rosenthal, A., 2010. Water and its influence on the lithosphere–asthenosphere boundary. Nature 467 (7314), 448–451.
Grégoire, M., Bell, D.R., Le Roex, A.P., 2003. Garnet lherzolites from the Kaapvaal Craton (South Africa): trace element evidence for a metasomatic history. J. Petrol. 44 (4), 629–657.
Griffin, W.L., Doyle, B.J., Ryan, C.G., Pearson, N.J., Suzanne, Y.O.R., Davies, R., Kivi, K., Van Achterbergh, E., Natapov, L.M., 1999. Layered mantle lithosphere in the Lac de Gras area, Slave craton: composition, structure and origin. J. Petrol. 40 (5), 705–727.
Griffin, W.L., O'reilly, S.Y., Afonso, J.C., Begg, G.C., 2009. The composition and evolution of lithospheric mantle: a re-evaluation and its tectonic implications. J. Petrol. 50 (7), 1185–1204.
Groppo, C., Rolfo, F., Castelli, D., Mosca, P., 2017. Metamorphic CO2 production in collisional orogens: petrological constraints from phase diagram modeling of Himalayan, scapolite-bearing, calc-silicate rocks in the NKC (F) MAS (T)-HC system. J. Petrol. 58 (1), 53–83.
Groppo, C., Rolfo, F., Frezzotti, M.L., 2022. CO2 outgassing during collisional orogeny is facilitated by the generation of immiscible fluids. Commun. Earth Environ. 3 (1), 1–11.
Harangi, S., Novák, A., Kiss, B., Seghedi, I., Lukács, R., Szarka, L., Wesztergom, V., Metwaly, M., Gribovszki, K., 2015. Combined magnetotelluric and petrologic constrains for the nature of the magma storage system beneath the Late Pleistocene Ciomadul volcano (SE Carpathians). J. Volcanol. Geoth. Res. 290, 82–96.
Hauser, F., Raileanu, V., Fielitz, W., Dinu, C., Landes, M., Bala, A., Prodehl, C., 2007. Seismic crustal, structure between the Transylvanian Basin, and the black sea, Romania. Tectonophysics 430 (1–4), 1–25.
Hermann, J., Lakey, S., 2021. Water transfer to the deep mantle through hydrous, Al-rich silicates in subduction zones. Geology 49 (8), 911–915.
Hurtig, E., Cermák, V., Haenel, R., Zui, V.I. (Eds.), 1992. Geothermal Atlas of Europe. Haack, Gotha.
Ionete, R.E., Popescu, R., Costinel, D., 2015. An isotopic survey of some mineral water resources in the Carpathian chain (Romania). Environ. Eng. Manag. J. 14 (10).
Ismail-Zadeh, A., Matenco, L., Radulian, M., Cloetingh, S., Panza, G., 2012. Geodynamics and intermediate-depth seismicity in Vrancea (the south-eastern Carpathians): current state-of-the art. Tectonophysics 530, 50–79.
Italiano, F., Kis, B.M., Baciu, C., Ionescu, A., Harangi, S., Palcsu, L., 2017. Geochemistry of dissolved gases from the eastern carpathians-Transylvanian basin boundary. Chem. Geol. 469, 117–128.
Jánosi, C., Szakáll, S., Kis, B.M., Kristály, F., Harangi, S., Péter, É., 2022. Minerals, mofettes, mineral waters and spa culture at Ciomadul. In: Ciomadul (Csomád), the Youngest Volcano in the Carpathians: Volcanism, Palaeoenvironment, Human Impact. Springer International Publishing, Cham, pp. 121–141.
Karátson, D., Telbisz, T., Dibacto, S., Lahitte, P., Szakács, A., Veres, D., Gertisser, R., Jánosi, C., Timár, G., 2019. Eruptive history of the late quaternary Ciomadul (csomád) volcano, east Carpathians, part II: magma output rates. Bull. Volcanol. 81 (4), 1–20.
Kennedy, B.M., Van Soest, M.C., 2007. Flow of mantle fluids through the ductile lower crust: helium isotope trends. Science 318 (5855), 1433–1436.
Kerrick, D.M., Caldeira, K., 1998. Metamorphic CO2 degassing from orogenic belts. Chem. Geol. 145 (3–4), 213–232.
Kind, R., Handy, M.R., Yuan, X., Meier, T., Kämpf, H., Soomro, R., 2017. Detection of a new sub-lithospheric discontinuity in Central Europe with S-receiver functions. Tectonophysics 700, 19–31.
Kis, B.M., Caracausi, A., Palcsu, L., Baciu, C., Ionescu, A., Futó, I., Sciarra, A., Harangi, S., 2019. Noble gas and carbon isotope systematics at the seemingly inactive Ciomadul volcano (Eastern-Central Europe, Romania): evidence for volcanic degassing. Geochem., Geophys., Geosyst. 20 (6), 3019–3043.
Kis, B.M., Baciu, C., Zsigmond, A.R., Kékedy-Nagy, L., Kármán, K., Palcsu, L., Máthé, I., Harangi, S., 2020. Constraints on the hydrogeochemistry and origin of the CO2-rich mineral waters from the Eastern Carpathians–Transylvanian Basin boundary (Romania). J. Hydrol. 591, 125311.
Knapp, J.H., Knapp, C.C., Raileanu, V., Mațenco, L., Mocanu, V., Dinu, C., 2005. Crustal constraints on the origin of mantle seismicity in the Vrancea Zone, Romania: the case for active continental lithospheric delamination. Tectonophysics 410 (1–4), 311–323.
Kovács, I., O'Neill, H.S.C., Hermann, J., Hauri, E.H., 2010. Site-specific infrared OH absorption coefficients for water substitution into olivine. Am. Mineral. 95 (2–3), 292–299.
Kovács, I., Patkó, L., Falus, G., Aradi, L.E., Szanyi, G., Gráczer, Z., Szabó, C., 2018. Upper mantle xenoliths as sources of geophysical information: the Perşani Mts. area as a case study. Acta Geodaetica et Geophysica 53 (3), 415–438.
Kovács, I.J., Liptai, N., Koptev, A., Cloetingh, S.A., Lange, T.P., Mațenco, L., Szakács, A., Radulian, M., Berkesi, M., Patkó, L., Molnár, G., Novák, A., Wesztergom, V., Szabó, C., Fancsik, T., 2021. The 'pargasosphere'hypothesis: looking at global plate tectonics from a new perspective. Global Planet. Change 204, 103547.
Kusakabe, M., Ohsumi, T., Aramaki, S., 1989. The Lake Nyos gas disaster: chemical and isotopic evidence in waters and dissolved gases from three Cameroonian crater lakes, Nyos, Monoun and Wum. J. Volcanol. Geoth. Res. 39 (2–3), 167–185.
Lange, T.P., Pálos, Z., Pósfai, M., Berkesi, M., Pekker, P., Szabó, Á., Cs, Szabó, Kovács, I. J., 2023. Nanoscale hydrous silicate melt inclusions at the clinopyroxene-amphibole interface in a mantle xenolith from the Perşani Mountains Volcanic Field. Lithos 454, 107210.
Laumonier, M., Karakas, O., Bachmann, O., Gaillard, F., Lukács, R., Seghedi, I., Menand, T., Harangi, S., 2019. Evidence for a persistent magma reservoir with large melt content beneath an apparently extinct volcano. Earth Planet Sci. Lett. 521, 79–90.
Lemonnier, C., Marquis, G., Perrier, F., Avouac, J.P., Chitrakar, G., Kafle, B., Sapkota, S., Gautam, U., Tiwari, D., Bano, M., 1999. Electrical structure of the Himalaya of central Nepal: high conductivity around the mid-crustal ramp along the MHT. Geophys. Res. Lett. 26 (21), 3261–3264.
Manning, C.E., 2004. The chemistry of subduction-zone fluids. Earth Planet Sci. Lett. 223 (1–2), 1–16.
Manning, C.E., Shock, E.L., Sverjensky, D.A., 2013. The chemistry of carbon in aqueous fluids at crustal and upper-mantle conditions: experimental and theoretical constraints. Rev. Mineral. Geochem. 75 (1), 109–148.
Martin, M., Wenzel, F., CALIXTO Working Group, 2006. High-resolution teleseismic body wave tomography beneath SE-Romania-II. Imaging of a slab detachment scenario. Geophys. J. Int. 164 (3), 579–595.
Marty, B., Zimmermann, L., 1999. Volatiles (He, C, N, Ar) in mid-ocean ridge basalts: assesment of shallow-level fractionation and characterization of source composition. Geochem. Cosmochim. Acta 63 (21), 3619–3633.
Mațenco, L., 2017. Tectonics and exhumation of Romanian Carpathians: inferences from kinematic and thermochronological studies. In: Landform Dynamics and Evolution in Romania. Springer, Cham, pp. 15–56.
Mațenco, L., Bertotti, G., Leever, K., Cloetingh, S.A.P.L., Schmid, S.M., Tărăpoancă, M., Dinu, C., 2007. Large-scale deformation in a locked collisional boundary: interplay between subsidence and uplift, intraplate stress, and inherited lithospheric structure in the late stage of the SE Carpathians evolution. Tectonics 26 (4).
Mațenco, L., Krezsek, C., Merten, S., Schmid, S., Cloetingh, S., Andriessen, P., 2010. Characteristics of collisional orogens with low topographic build-up: an example from the Carpathians. Terra. Nova 22 (3), 155–165.
Méjean, P., Pinti, D.L., Kagoshima, T., Roulleau, E., Demarets, L., Poirier, A., Takahata, N., Sano, Y., Larocque, M., 2020. Mantle helium in Southern Quebec groundwater: a possible fossil record of the New England hotspot. Earth Planet Sci. Lett. 545, 116352.
Merten, S., Mațenco, L., Foeken, J.P.T., Stuart, F.M., Andriessen, P.A.M., 2010. From nappe stacking to out-of-sequence postcollisional deformations: Cretaceous to Quaternary exhumation history of the SE Carpathians assessed by low-temperature thermochronology. Tectonics 29 (3).
Molnár, K., Czuppon, G., Palcsu, L., Benkó, Z., Lukács, R., Kis, B.M., Németh, B., Harangi, S., 2021. Noble gas geochemistry of phenocrysts from the Ciomadul volcanic dome field (Eastern Carpathians). Lithos 394, 106152.
Molnár, K., Harangi, S., Lukács, R., Dunkl, I., Schmitt, A.K., Kiss, B., Garamhegyi, T., Seghedi, I., 2018. The onset of the volcanism in the Ciomadul volcanic dome complex (eastern Carpathians): eruption chronology and magma type variation. J. Volcanol. Geoth. Res. 354, 39–56.
Mook, W., Rozanski, K., 2000. Environmental Isotopes in the Hydrological Cycle. IAEA Publish, p. 39.
Murgeanu, G., Dumitrescu, I., Mirăuă, O., Săndulescu, M., Tefănescu, M., Bandrabur, T., 1968. Geological Map of Romania 1 : 200.000. Sheet Bacau. Geol. Inst., Bucharest.
Mutlu, H., Güleç, N., Hilton, D.R., 2008. Helium–carbon relationships in geothermal fluids of western Anatolia, Turkey. Chem. Geol. 247 (1–2), 305–321.
Necea, D., Juez-Larré, J., Mațenco, L., Andriessen, P.A., Dinu, C., 2021. Foreland migration of orogenic exhumation during nappe stacking: inferences from a high-resolution thermochronological profile over the Southeast Carpathians. Global Planet. Change 200, 103457.

Newton, R.C., 1986. Fluids of granulite facies metamorphism. In: Fluid—Rock Interactions during Metamorphism. Springer, New York, pp. 36–59.
Newton, R.C., Manning, C.E., 2008. Thermodynamics of SiO2–H2O fluid near the upper critical end point from quartz solubility measurements at 10 kbar. Earth Planet Sci. Lett. 274 (1–2), 241–249.
Niedermann, S., 2002. Cosmic-ray-produced noble gases in terrestrial rocks: dating tools for surface processes. Rev. Mineral. Geochem. 47 (1), 731–784.
Niida, K., Green, D.H., 1999. Stability and chemical composition of pargasitic amphibole in MORB pyrolite under upper mantle conditions. Contrib. Mineral. Petrol. 135 (1), 18–40.
Panaiotu, C.G., Jicha, B.R., Singer, B.S., Ţugui, A., Seghedi, I., Panaiotu, A.G., Necula, C., 2013. 40Ar/39Ar chronology and paleomagnetism of quaternary basaltic lavas from the perşani mountains (east Carpathians). Phys. Earth Planet. Inter. 221, 1–14.
Papp, L., Palcsu, L., Major, Z., Rinyu, L., Tóth, I., 2012. A mass spectrometric line for tritium analysis of water and noble gas measurements from different water amounts in the range of microlitres and millilitres. Isot. Environ. Health Stud. 48 (4), 494–511.
Papp, L., Palcsu, L., Veres, M., Pintér, T., 2016. A new dissolved gas sampling method from primary water of the Paks Nuclear Power Plant, Hungary. Nucl. Eng. Des. 300, 536–540.
Pécskay, Z., Lexa, J., Szakács, A., Seghedi, I., Balogh, K., Konecny, V., Zelenka, T., Kovacs, M., Póka, T., Fülöp, A., Márton, E., Panaiotu, C., Cvetkovic, V., 2006. Geochronology of Neogene magmatism in the Carpathian arc and intra-Carpathian area. Geologica Carpathica-Bratislava- 57 (6), 511.
Petrescu, L., Borleanu, F., Radulian, M., Ismail-Zadeh, A., Maţenco, L., 2021. Tectonic regimes and stress patterns in the Vrancea Seismic Zone: insights into intermediate-depth earthquake nests in locked collisional settings. Tectonophysics 799, 228688.
Pili, E., Kennedy, B.M., Conrad, M.E., Gratier, J.P., 2011. Isotopic evidence for the infiltration of mantle and metamorphic CO2–H2O fluids from below in faulted rocks from the San Andreas Fault system. Chem. Geol. 281 (3–4), 242–252.
Popa, M., Radulian, M., Szakács, A., Seghedi, I., Zaharia, B., 2012. New seismic and tomography data in the southern part of the Harghita Mountains (Romania, Southeastern Carpathians): connection with recent volcanic activity. Pure Appl. Geophys. 169 (9), 1557–1573.
Popescu, E., Placinta, A.O., Borleasnu, F., Radulian, M., 2017. Repeated earthquakes in the Vrancea subcrustal source and source scaling. In: IOP Conference Series: Earth and Environmental Science, vol. 95. IOP Publishing, 032005. No. 3.
Précigout, J., Stünitz, H., Villeneuve, J., 2019. Excess water storage induced by viscous strain localization during high-pressure shear experiment. Sci. Rep. 9 (1), 1–9.
Radulian, M., Popa, M., Cărbunar, O., Rogozea, M., 2008. Seismicity patterns in Vrancea and predictive features. Acta Geod. Geophys. Hung. 43 (2–3), 163–173.
Randazzo, P., Caracausi, A., Aiuppa, A., Cardellini, C., Chiodini, G., D'Alessandro, W., Vigni, L.L., Papic, P., Marinkovic, G., Ionescu, A., 2021. Active degassing of deeply sourced fluids in central Europe: new evidences from a geochemical study in Serbia. Geochem., Geophys., Geosyst. 22 (11), e2021GC010017.
Reiners, P.W., Brandon, M.T., 2006. Using thermochronology to understand orogenic erosion. Annu. Rev. Earth Planet Sci. 34 (1), 419–466.
Ren, Y., Stuart, G.W., Houseman, G.A., Dando, B., Ionescu, C., Hegedüs, E., Radovanović, S., Shen, Y., South Carpathian Project Working Group, 2012. Upper mantle structures beneath the Carpathian–Pannonian region: implications for the geodynamics of continental collision. Earth Planet Sci. Lett. 349, 139–152.
Roban, R.D., Ducea, M.N., Maţenco, L., Panaiotu, G.C., Profeta, L., Krézsek, C., Melinte-Dobrinescu, M.-C., Anastasiu, N., Dimofte, D., Apotrosoaei, V., Francovschi, I., 2020. Lower Cretaceous provenance and sedimentary deposition in the Eastern Carpathians: Inferences for the evolution of the subducted oceanic domain and its European passive continental margin. Tectonics 39 (7), e2019TC005780. https://agupubs.onlinelibrary.wiley.com/doi/epdf/10.1029/2019TC005780.
Roban, R.D., Melinte-Dobrinescu, M.C., 2012. Lower cretaceous lithofacies of the black shales rich audia formation, Tarcău nappe, eastern Carpathians: genetic significance and sedimentary palaeoenvironments. Cretac. Res. 38, 52–67.
Rogie, J.D., Kerrick, D.M., Chiodini, G., Frondini, F., 2000. Flux measurements of nonvolcanic $CO_2$ emission from some vents in central Italy. J. Geophys. Res. Solid Earth 105 (B4), 8435–8445.
Rozanski, K., Araguás-Araguás, L., Gonfiantini, R., 2013. Isotopic Patterns in Modern Global Precipitation. https://doi.org/10.1029/gm078p0001.
Russo, R.M., Mocanu, V., Radulian, M., Popa, M., Bonjer, K.P., 2005. Seismic attenuation in the Carpathian bend zone and surroundings. Earth Planet Sci. Lett. 237 (3–4), 695–709.
Saintot, A., Stephenson, R.A., Stovba, S., Brunet, M.F., Yegorova, T., Starostenko, V., 2006. The evolution of the southern margin of eastern Europe (eastern European and scythian platforms) from the latest precambrian-early palaeozoic to the early cretaceous. Geological Society, London, Memoirs 32 (1), 481–505.
Sano, Y., Marty, B., 1995. Origin of carbon in fumarolic gas from island arcs. Chem. Geol. 119 (1–4), 265–274.
Sano, Y., Wakita, H., 1985. Geographical distribution of 3He/4He ratios in Japan: implications for arc tectonics and incipient magmatism. J. Geophys. Res. Solid Earth 90 (B10), 8729–8741.
Seghedi, A., Berza, T., Iancu, V., Marunţiu, M., Gheorghe, O.A.I.E., 2005. Neoproterozoic terranes in the Moesian basement and in the alpine danubian nappes of the south Carpathians. Geol. Belg. 8 (4), 4–19. https://popups.uliege.be/1374-8505/index.php?id=746.
Seghedi, I., Popa, R.G., Panaiotu, C.G., Szakács, A., Pécskay, Z., 2016. Short-lived eruptive episodes during the construction of a Na-alkalic basaltic field (Perşani Mountains, SE Transylvania, Romania). Bull. Volcanol. 78 (10), 1–16.
Seghedi, I., Besutiu, L., Mirea, V., Zlagnean, L., Popa, R.G., Szakács, A., Atanasiu, L., Pomeran, M., Vişan, M., 2019. Tectono-magmatic characteristics of post-collisional magmatism: case study East Carpathians, Călimani-Gurghiu-Harghita volcanic range. Phys. Earth Planet. Inter. 293, 106270.
Shcheka, S.S., Wiedenbeck, M., Frost, D.J., Keppler, H., 2006. Carbon solubility in mantle minerals. Earth Planet Sci. Lett. 245 (3–4), 730–742.
Sheppard, S.M., 1986. Characterization and isotopic variations in natural waters. In: Stable Isotopes in High Temperature Geological Processes. De Gruyter, pp. 165–184.
Siebenaller, L., Boiron, M.C., Vanderhaeghe, O., Hibsch, C., Jessell, M.W., Andre-Mayer, A.S., France-Lanord, C., Photiades, A., 2013. Fluid record of rock exhumation across the brittle–ductile transition during formation of a Metamorphic Core Complex (Naxos Island, Cyclades, Greece). J. Metamorph. Geol. 31 (3), 313–338.
Sleep, N.H., Blanpied, M.L., 1992. Creep, compaction and the weak rheology of major faults. Nature 359 (6397), 687–692.
Sóki, E., Csige, I., 2016. Radon in the dry carbon dioxide spa of Mátraderecske, Hungary. Nukleonika 61 (3), 245–249.
Szabó, C., Bodnar, R.J., 1996. Changing magma ascent rates in the Nograd-Gomor volcanic field northern Hungary southern Slovakia: evidence from CO2-rich fluid inclusions in metasomatized upper mantle xenoliths. Petrology 4 (3), 240–249.
Sterner, S.M., Bodnar, R.J., 1991. Synthetic fluid inclusions; X, Experimental determination of PVTX properties in the $CO_2$-$H_2O$ system to 6 kb and 700 °C. Am. J. Sci. 291 (1), 1–54.
Szabó, Á., Berkesi, M., Aradi, L.E., Szabó, C., 2019. Traces of metasomatism beneath the Eastern Transylvanian Basin: evidence from upper mantle xenoliths. In: Geophysical Research Abstracts, vol. 21.
Szakács, A., 2021. Precursor-based earthquake prediction Research: proposal for a paradigm-shifting strategy. Front. Earth Sci. 670.
Szakács, A., Seghedi, I., 1995. Time-space evolution of neogene–quaternary volcanism in the calimani–Gurghiu–Harghita volcanic chain. Rom. J. Stratigr. 76, 24.
Szakács, A., Seghedi, I., Pécskay, Z., Mirea, V., 2015. Eruptive history of a low-frequency and low-output rate pleistocene volcano, Ciomadul, south Harghita Mts., Romania. Bull. Volcanol. 77 (2), 1–19.
Tari, G., Dicea, O., Faulkerson, J., Georgiev, G., Popov, S., Stefanescu, M., Weir, G., 1997. AAPG Memoir 68: Regional and Petroleum Geology of the Black Sea and Surrounding Region (Chapter 6): Cimmerian and Alpine Stratigraphy and Structural Evolution of the Moesian Platform (Romania/Bulgaria).
Tiliţă, M., Lenkey, L., Maţenco, L., Horváth, F., Surányi, G., Cloetingh, S., 2018. Heat flow modelling in the Transylvanian basin: implications for the evolution of the intra-Carpathians area. Global Planet. Change 171, 148–166.
Tingle, T.N., Green, H.W., 1987. Carbon solubility in olivine: implications for upper mantle evolution. Geology 15 (4), 324–326.
Tondi, R., Achauer, U., Landes, M., Davi, R., Besutiu, L., 2009. Unveiling seismic and density structure beneath the Vrancea seismogenic zone, Romania. J. Geophys. Res. Solid Earth 114 (B11).
Túri, M., Saadi, R., Marah, H., Temovski, M., Molnár, M., Palcsu, L., 2020. Paleotemperature reconstruction using environmental isotopes and noble gases in groundwater in Morocco. Hydrogeol. J. 28, 973–986.
Upton, P., Caldwell, T.G., Chamberlain, C.P., Craw, D., James, Z., Jiracek, G.J., Koons, P.O., Wannamaker, P.E., 2000. Fluids in a backthrust regime (southern Alps, New Zealand). J. Geochem. Explor. 69, 517–521.
Upton, P., Craw, D., Caldwell, T.G., Koons, P.O., James, Z., Wannamaker, P.E., Jiracek, G.J., Chamberlain, C.P., 2003. Upper crustal fluid flow in the outboard region of the Southern Alps, New Zealand. Geofluids 3 (1), 1–12.
Vaselli, O., Downes, H., Thirlwall, M., Dobosi, G., Coradossi, N., Seghedi, I., Szakács, A., Vannucci, R., 1995. Ultramafic xenoliths in Plio-Pleistocene alkali basalts from the Eastern Transylvanian Basin: depleted mantle enriched by vein metasomatism. J. Petrol. 36 (1), 23–53.
Vaselli, O., Minissale, A., Tassi, F., Magro, G., Seghedi, I., Ioane, D., Szakács, A., 2002. A geochemical traverse across the Eastern Carpathians (Romania): constraints on the origin and evolution of the mineral water and gas discharges. Chem. Geol. 182 (2–4), 637–654.
Vauchez, A., Tommasi, A., Mainprice, D., 2012. Faults (shear zones) in the Earth's mantle. Tectonophysics 558, 1–27.
Veliciu, S., Demetrescu, C., 1979. Heat flow in Romania and some relations to geological and geophysical features. In: Terrestrial Heat Flow in Europe. Springer Berlin Heidelberg, pp. 253–260.
Vosteen, H.-D., Schellschmidt, R., 2003. Phys. Chem. Earth 28 (9–11), 499–509.
Winter, J.D., 2014. Principles of Igneous and Metamorphic Petrology, 2ndEdn.
Yardley, B.W., Bodnar, R.J., 2014. Fluids in the continental crust. Geochemical Perspectives 3 (1), 1–2.
Zhang, M., Zhang, L., Zhao, W., Guo, Z., Xu, S., Sano, Y., Li, Y., 2021. Metamorphic CO2 emissions from the southern Yadong-Gulu rift, Tibetan Plateau: Insights into deep carbon cycle in the India-Asia continental collision zone. Chem. Geol. 584, 120534.